Inorg. Chem. **2003**, *42*, 767−784

Structure and Reactivity of a Chromium(V) Glutathione Complex[1]

Aviva Levina, Lianbo Zhang, and Peter A. Lay*

Centre for Heavy Metal Research, School of Chemistry, University of Sydney, Sydney 2006 NSW, Australia

Received October 15, 2002

Chromium(V) glutathione complexes are among the likely reactive intermediates in Cr(VI)-induced genotoxicity and carcinogenicity. The first definitive structure of one such complex, $[Cr^{V}O(LH_2)_2]^{3-}$ (**I**; LH_5 = glutathione = GSH), isolated from the reaction of Cr(VI) with excess GSH at pH 7.0 (O'Brien, P.; Pratt, J.; Swanson, F. J.; Thornton, P.; Wang, G. *Inorg. Chim. Acta* **1990**, *169*, 265–269), has been determined by a combination of electrospray mass spectrometry (ESMS), X-ray absorption spectroscopy (XAS), EPR spectroscopy, and analytical techniques. In addition, Cr(V) complexes of GSH ethyl ester (γ-Glu-Cys-GlyOEt) have been isolated and characterized by ESMS, and Cr(III) products of the Cr(VI) + GSH reaction have been isolated and characterized by ESMS and XAS. The thiolato and amido groups of the Cys residue in GSH are responsible for the Cr(V) binding in **I**. The Cr–ligand bond lengths, determined from multiple-scattering XAFS analysis, are as follows: 1.61 Å for the oxo donor; 1.99 Å for the amido donors; and 2.31 Å for the thiolato donors. A significant electron withdrawal from the thiolato groups to Cr(V) in **I** was evident from the XANES spectra. Rapid decomposition of **I** in aqueous solutions (pH = 1–13) occurs predominantly by ligand oxidation with the formation of Cr(III) complexes of GSH and GSSG. Maximal half-lives of the Cr(V) species (40–50 s at [Cr] = 1.0 mM and 25 °C) are observed at pH 7.5–8.0. The experimental data are in conflict with a recent communication (Gaggelli, E.; Berti, F.; Gaggelli, N.; Maccotta, A.; Valensin, G. *J. Am. Chem. Soc.* **2001**, *123*, 8858–8859) on the formation of a Cr(V) dimer as a major product of the Cr(VI) + GSH reaction, which may have resulted from misinterpretation of the ESMS and NMR spectroscopic data.

Introduction

Chromium(VI) is an established carcinogen[2,3] and a potent mutagen for bacterial and mammalian cells.[4,5] The generally accepted mechanism for the biological action of Cr(VI)[6−8] includes the following: (i) uptake by cells through anion channels (for $[CrO_4]^{2-}$) or through phagocytosis (for insoluble chromates); (ii) intracellular reduction of Cr(VI) to Cr(III) with the formation of reactive Cr(V), Cr(IV), and free radical intermediates, capable of damaging DNA; (iii) stabilization of Cr(V) and Cr(IV) species by intracellular ligands such as 1,2-diolates and 2-hydroxycarboxylates; and (iv) formation of kinetically inert Cr(III) complexes with biological macromolecules as the products of Cr(VI) reductions. Glutathione (GSH) and ascorbate are the most likely intracellular reductants of Cr(VI);[9,10] therefore, their ability to stabilize the Cr(V) oxidation state[11−16] is important in

* To whom correspondence should be addressed. E-mail: p.lay@chem.usyd.edu.au.

(1) Abbreviations: Ala = L-alanine; Cys = L-cysteine; DTPA = diethylenetriaminepentaacetic acid, DMF = dimethylformamide; DMPO = dimethyl-1-pyrroline *N*-oxide; $ehbaH_2$ = 2-ethyl-2-hydroxybutanoic acid; DMSO = dimethyl sulfoxide; ESMS = electrospray mass spectrometry; FT = Fourier transform; Glu = L-glutamic acid; Gly = glycine; GSH = LH_5 = glutathione (γ-Glu-Cys-Gly); GSHOEt = glutathione ethyl ester (γ-Glu-Cys-GlyOEt); GSSG = LLH_8 = oxidized glutathione; HEPES = *N*-[2-hydroxyethyl]-piperazine-*N*′-[2-ethanesulfonic acid]; LW = line width; MS = multiple scattering; qaH_2 = quinic acid = (1*R*,3*R*,4*R*,5*R*)-1,3,4,5-tetrahydroxycyclohexanecarboxylic acid; SHF = superhyperfine; SS = single scattering; TGA = thermogravimetric analysis; XAFS = X-ray absorption fine structure; XANES = X-ray absorption near-edge structure; and XAS = X-ray absorption spectroscopy.

(2) *IARC. Monographs on the Evaluation of the Carcinogenic Risk of Chemicals to Humans. Vol.49. Chromium, Nickel and Welding*; International Agency on the Research of Cancer: Lyon, France, 1990.
(3) Gibb, H. J.; Lees, P. S. J.; Pinsky, P. F.; Rooney, B. C. *Am. J. Ind. Med.* **2000**, *38*, 115−126.
(4) De Flora, S.; Camoirano, A.; Bagnasco, M.; Zanacchi, P. In *Handbook of Metal−Ligand Interactions in Biological Fluids. Bioinorganic Medicine*; Berthon, G., Ed.; Marcel Dekker: New York, 1995; Vol. 2, pp 1020−1036 and references therein.
(5) Dillon, C. T.; Lay, P. A.; Bonin, A. M.; Cholewa, M.; Legge, G. J. F.; Collins, T. J.; Kostka, K. L. *Chem. Res. Toxicol.* **1998**, *11*, 119−129 and references therein.
(6) Connett, P. H.; Wetterhahn, K. E. *Struct. Bonding (Berlin)* **1983**, *54*, 93−124.
(7) Codd, R.; Dillon, C. T.; Levina, A.; Lay, P. A. *Coord. Chem. Rev.* **2001**, *216−217*, 537−582 and references therein.
(8) Levina, A.; Codd, R.; Dillon, C. T.; Lay, P. A. *Prog. Inorg. Chem.* **2003**, *51*, 145−250 and references therein.
(9) Connett, P. H.; Wetterhahn, K. E. *J. Am. Chem. Soc.* **1985**, *107*, 4282−4288.

10.1021/ic020621o CCC: $25.00
Published on Web 01/11/2003

relation to Cr(VI)-induced genotoxicity and carcinogenicity.[17,18] Formation of Cr(V) complexes during the reactions of Cr(VI) with GSH has been studied by EPR spectroscopy;[11−14] however, the nature of these Cr(V) species remained unclear.[19] Although the isolation of a Cr(V)-containing solid from the Cr(VI) + GSH reaction has been reported,[20,21] this product was only partially characterized,[21] because of the instability of Cr(V) in solutions, which has precluded its purification and crystallization to date.

The development in the last 10 years of new methods for characterization of unstable metal complexes, including X-ray absorption spectroscopy (XAS)[22] and electrospray mass spectrometry (ESMS),[23] has prompted us to reinvestigate the Cr(V) intermediates formed in the Cr(VI) + GSH reaction. Preliminary results of these studies have been reported,[7] although the proposed structure of a Cr(V)−GSH complex[7] has been subsequently reassigned (see Discussion). At the time that the current work was being completed, Gaggelli et al.[24] reported the characterization of the Cr(V) species formed in the Cr(VI) + GSH reaction under a different set of conditions, using a combination of EPR and NMR spectroscopies and ESMS. However, their conclusions were erroneous, because these conditions did not result in the production of a Cr(V) species as a major product (see Discussion section). In the current work, a definitive structure of a Cr(V)−GSH complex, $[Cr^{V}O(LH_2)_2]^{3-}$ (LH_5 = GSH), has been established by a combination of ESMS, XAS, EPR spectroscopy, and analytical techniques. The reactivity of $[Cr^{V}O(LH_2)_2]^{3-}$ in aqueous solutions has been studied in relation to the possible roles of Cr(V)−GSH complexes in Cr(VI)-induced genotoxicity. This is the first detailed study of the structure and reactivity of a Cr(V) complex with a ubiquitous biological ligand, GSH.

Experimental Section

Caution! Cr(VI) compounds are human carcinogens,[2,3] and the Cr(V) complexes are mutagenic, rapidly cleave DNA at micromolar concentrations, and are potential carcinogens.[5,25] Appropriate precautions should be taken to avoid skin contact and inhalation of Cr(VI) and Cr(V) solutions and dusts.

Reagents. The following reagents of analytical or higher purity grade were used without purification: glutathione (reduced form), 2-ethyl-2-hydroxybutanoic acid, 5,5′-dithiobis-2-nitrobenzoic acid (Ellman's reagent), DMF, DMPO, DTPA, NaOH, D_2O (≥99.96%), and BN (all Aldrich); glutathione (oxidized form) and glutathione ethyl ester (all Sigma); $Na_2CrO_4 \cdot 4H_2O$, $NaClO_4 \cdot H_2O$, $NaBH_4$, $(NH_4)_2Fe(SO_4)_2 \cdot 6H_2O$, CH_3COOH, HNO_3, $HClO_4$, NH_3 (aqueous solution, 32% w/v), HCl (aqueous solution, 35% w/v), NaCl, and NaI (all Merck); L-ascorbic acid (ICN Biomedicals); HEPES (Research Organics); *sym*-diphenylcarbazide (Fluka); and H_2O_2 (30% aqueous solution, BDH chemicals). A model Cr(V) complex, $Na[Cr^{V}O(ehba)_2] \cdot H_2O$, was synthesized by the method of Krumpolc and Roček,[26] and its purity was confirmed by ESMS and UV−vis and EPR spectroscopies. Water was purified by the Milli-Q technique.

General Methods. Stock solutions of the buffers (0.50 M HEPES + NaOH, pH 7.40, or 1.0 M CH_3COOH + NH_3, pH 4.0−10.0) were treated by Chelex 100 chelating resin (BioRad) and stored at 4 °C. Concentrations of the catalytic metals (Fe(III) and Cu(II)) in the purified buffers, determined by Buettner's ascorbate method,[27] were <0.5 μM. Stock solutions of GSH were prepared daily and stored under Ar. Solutions of Cr(V)−GSH, Cr(V)−GSHOEt, or Cr(III)−GSH were prepared from the solids within 30 s before use, unless otherwise stated. The pH values of the reaction solutions were adjusted using high purity NaOH (99.99%, Aldrich) and verified immediately before and after the reactions, using a HI 9023 ionometer with a HI 1038 glass/Ag/AgCl electrode. The reaction solutions were saturated with high purity Ar (BOC gases); residual $[O_2]$ in the solutions was <0.01 mM (measured with a Clark-type oxygen electrode, as described previously).[28]

Isolation of the Cr(V)−GSH, Cr(V)−GSHOEt, and Cr(III)−GSH Complexes. A green Cr(V)-containing solid (Cr(V)−GSH) was isolated according to the method of O'Brien et al.[21] Aqueous solutions of GSH (5.0 mL, 1.0 M, pH adjusted to 7.0 with NaOH) and Na_2CrO_4 (5.0 mL, 0.10 M) were mixed at 0 °C and allowed to react for 150 s before the addition of ice-cold MeOH (60 mL). The formed precipitate was filtered, washed with MeOH, and dried under vacuum. The data of elemental analyses for the Cr(V)−GSH complex are given in the Results section. The same method was used to isolate a Cr(III)−GSH complex (purple solid; 2.9% Cr w/w), except that the Cr(VI) + GSH reaction was allowed to proceed for 2 h at 22 °C. A green solid (Cr(V)−GSHOEt; 2.2% Cr w/w) was isolated from the Cr(VI) + GSHOEt reaction, using the same method as for the isolation of Cr(V)−GSH, but with 10-fold smaller quantities (mol) of the reagents. Attempts to isolate Cr(V)−containing solids from the reactions of Cr(VI) with other thiols, related to GSH, have so far been unsuccessful. The solid samples of Cr(V)−GSH, Cr(V)−GSHOEt, and Cr(III)−GSH were stored for up to a year at −20 °C, protected from light and moisture. No significant changes in ESMS and EPR and UV−vis spectra of the samples were observed during this time.

Analytical Methods. Concentrations of Cr(V)−GSH, Cr(V)−GSHOEt, or Cr(III)−GSH in the reaction mixtures were determined from the Cr content in the samples, which was measured by two independent methods. In the first, the samples were digested with

(10) Connett, P. H.; Wetterhahn, K. E. *J. Am. Chem. Soc.* **1986**, *108*, 1842−1847.
(11) O'Brien, P.; Barrett, J.; Swanson, F. *Inorg. Chim. Acta* **1985**, *108*, L19−L20.
(12) Goodgame, D. M. L.; Joy, A. M. *J. Inorg. Biochem.* **1986**, *26*, 219−224.
(13) Kitagawa, S.; Seki, H.; Kametani, F. Sakurai, H. *Inorg. Chim. Acta* **1988**, *152*, 251−255.
(14) Zhang, L.; Lay, P. A. *J. Am. Chem. Soc.* **1996**, *118*, 12624−12637 and references therein.
(15) Zhang, L.; Lay, P. A. *Aust. J. Chem.* **2000**, *53*, 7−13.
(16) Zhang, L. Ph.D. Thesis, University of Sydney, 1998.
(17) Kortenkamp, A.; Casadevall, M.; Da Cruz Fresco, P.; Shayer, R. O. J. *NATO ASI Ser., Ser. 2* **1997**, *26*, 15−34 and references therein.
(18) Stearns, D. M.; Wetterhahn, K. E. *NATO ASI Ser., Ser. 2* **1997**, *26*, 55−72 and references therein.
(19) Barr-David, G.; Charara, M.; Codd, R.; Farrell, R. P.; Irwin, J. A.; Lay, P. A.; Bramley, R.; Brumby, S.; Ji, J.-Y.; Hanson, G. R. *J. Chem. Soc., Faraday Trans.* **1995**, *91*, 1207−1216.
(20) Shi, X.; Dalal, N. S. *Biochem. Biophys. Res. Commun.* **1988**, *156*, 137−142.
(21) O'Brien, P.; Pratt, J.; Swanson, F. J.; Thornton, P.; Wang, G. *Inorg. Chim. Acta* **1990**, *169*, 265−269.
(22) Penner-Hahn, J. E. *Coord. Chem. Rev.* **1999**, *190−192*, 1101−1123.
(23) Henderson, W.; Nicholson, B. K.; McCaffrey, L. J. *Polyhedron* **1998**, *17*, 4291−4313.
(24) Gaggelli, E.; Berti, F.; Gaggelli, N.; Maccotta, A.; Valensin, G. *J. Am. Chem. Soc.* **2001**, *123*, 8858−8859.
(25) Levina, A.; Barr-David, G.; Codd, R.; Lay, P. A.; Dixon, N. E.; Hammershøi, A.; Hendry, P. *Chem. Res. Toxicol.* **1999**, *12*, 371−381 and references therein.
(26) Krumpolc, M.; Roček, J. *J. Am. Chem. Soc.* **1979**, *101*, 3206−3209.
(27) Buettner, G. R. *Methods Enzymol.* **1990**, *186*, 125−127.
(28) Lay, P. A.; Levina, A. *J. Am. Chem. Soc.* **1998**, *120*, 6704−6714.

70% HNO_3 and diluted with 0.10 M HCl, and Cr concentration was determined by C_2H_2/air flame AAS, using a Varian SpecAA-800 spectrometer, calibrated with standard Cr(III) solutions for AAS (Aldrich). In the second method, the samples (~1 mM) were reacted with 0.10 M H_2O_2 in 1.0 M NaOH at 100 °C for 15 min, and the concentration of the formed Cr(VI) was determined by UV−vis spectroscopy ($\epsilon = 4.81 \times 10^3$ M^{-1} cm^{-1} at 372 nm).[29] The results from both methods agreed within the experimental error (5%). Concentrations of Cr(VI) and thiol groups in the reaction mixtures were determined with diphenylcarbazide ($\epsilon = 4.2 \times 10^4$ M^{-1} cm^{-1} at 540 nm)[30] and Ellman's reagent ($\epsilon = 1.36 \times 10^4$ M^{-1} cm^{-1} at 412 nm),[31] respectively, as described previously;[32] calibrations were performed by a standard addition method to exclude the influence of the other components of the reaction mixtures. For the determination of total sulfur (GSH + GSSG), disulfide groups were reduced to thiol groups with $NaBH_4$ prior to the determination with Ellman's reagent.[33] A Hewlett-Packard HP 8452A diode-array spectrophotometer was used for UV−vis spectroscopic measurements. Determination of [Na^+] was performed with a Sherwood 410 flame photometer, using NaCl as a standard. Elemental analyses (C, H, N, S) were performed by the Australian National University Microanalytical Unit, using a Carlo Erba 1106 automatic analyzer, on the basis of chromatographic analyses of the combustion products. The TGA data were obtained using a TGA 2950 analyzer (TA Instruments) by heating the samples in an atmosphere of high purity N_2 (BOC gases) from 20 to 500 °C at 10 °C/min. Magnetic susceptibility was measured on a Sherwood Scientific magnetic susceptibility balance. The balance was calibrated with $(NH_4)_2Fe(SO_4)_2 \cdot 6H_2O$, and diamagnetic corrections for the constituent atoms were calculated from the literature.[34]

Electrospray Mass Spectrometry. The ESMS analyses were performed using a Finnigan LCQ mass spectrometer; typical experimental settings were as follows: sheath gas (N_2) pressure, 60 psi; spray voltage, 5.0 kV; capillary temperature, 200 °C; capillary voltage, 19 V; tube lens offset, 25 V; *m*/*z* range, 100−2000 (both in positive- and negative-ion modes). Analyzed aqueous solutions (5 μL, 0.50−1.0 mM Cr) were injected into a flow of H_2O/MeOH (1:1 v/v, flow rate 0.20 mL min^{-1}). This injection method allowed a mass spectrum to be obtained within ~30 s after dissolution of the sample, which is critical for the unstable Cr(V) species, as well as increased the sensitivity by providing optimal spraying conditions.[35,36] No qualitative differences in the ESMS spectra were observed when H_2O was used as the eluent instead of H_2O/MeOH. Acquired spectra were the averages of 10 scans (scan time 10 ms). Simulations of the mass spectra were performed using *IsoPro* software.[37]

EPR Spectroscopy. Room temperature (22 ± 1 °C) X-band EPR spectra were acquired on a Bruker EMX spectrometer; calibrations of the magnetic field and the microwave frequency were performed with an EMX 035 NMR gaussmeter and an EMX 048T microwave bridge controller, respectively. Room-temperature Q-band EPR spectra, as well as low temperature (10 ± 1 K) X-band EPR spectra, were acquired on a Bruker ESP 300 spectrometer equipped with a BVT 2000 variable temperature unit and an E900 continuous flow liquid He cryostat (Oxford Instruments). Quartz capillaries and a Wilmad quartz flat cell were used for the solids and solutions, respectively. Typical settings of the EPR spectrometers were the following: center field, 3480 G (X-band) or 12100 G (Q-band); sweep width, 200 G (for the solutions), 1000 G (solids at 22 °C), or 6900 G (solids at 10 K); resolution, 1024 points; microwave power, 2.0 mW (X-band at 22 °C), 6.3 mW (Q-band), or 0.20 W (X-band at 10 K); microwave frequency, ~9.67 GHz (X-band at 22 °C), ~9.46 GHz (X-band at 10 K), or ~33.7 GHz (Q-band); modulation frequency, 100 kHz; modulation amplitude, 0.10−5.0 G; time constant, 20.48 ms; receiver gain, 10^2-10^5; and number of scans, 5−10. Time-dependent EPR spectra in solutions (X-band, 22 °C) were measured without removing the cell from the cavity of the EPR spectrometer. The EPR spectra were processed with *WinEPR*,[38] the g_{iso} values and line widths (LW) of the signals were determined by simulation of the spectra with *WinSim*,[39] and second-order corrections were applied in the simulations.

Kinetic Studies. Stability and ligand-exchange reactions of the isolated Cr(V)−GSH complex, as well as the kinetics of the Cr(VI) + GSH reactions, were studied using a HP 8452 A diode-array spectrophotometer (time scale, 30 s to 2 h; linear time base; λ = 300−800 nm; resolution, 2 nm; integration time, 0.2 s; and number of spectra, 10−60). A constant temperature (5.0 ± 0.2, 22.0 ± 0.1, 25.0 ± 0.1, or 27.0 ± 0.1 °C) was maintained using a HP 89090A temperature control unit. Reactions of Cr(V)−GSH were initiated by dissolution of the solid compound in the appropriate buffer solution (freshly prepared, Ar-saturated and thermostated at the required temperature). Time-dependent UV−vis spectra were processed by global kinetic analysis techniques,[40] using *Pro-Kineticist* software,[41] as described previously.[28,42,43]

X-ray Absorption Spectroscopy and Data Processing. Chromium K-edge spectra of the Cr(V)−GSH and Cr(III)−GSH complexes were recorded on the Australian National Beamline Facility (beamline 20B) at the Photon Factory, Tsukuba, Japan. The beam energy was 2.5 GeV, and the beam current, 300−400 mA. A Si[111] double-crystal monochromator was detuned by 50%. The spectra were recorded in transmission mode, using N_2/He-filled ionization chambers. Solid samples were mixed with BN (mass ratio 1:1) and pressed into 0.5-mm pellets supported in an Al spacer between two 63.5-μm Kapton tape windows. The sample temperature was maintained at 10 ± 1 K using a closed-cycle He CryoIndustries REF-1577-D22 cryostat. Collection of XAS data at low temperature minimized sample photodamage, improved the signal-to-noise ratio, and maximized the MS contributions to the XAFS spectrum.[44] The spectra were averaged from three scans taken at different positions on the sample; no color changes at irradiated spots were observed, and the edge energies differed by <0.1 eV between the scans. The energy scale was calibrated using

(29) Haupt, G. W. *Natl. Bur. Stand. Circ. (U. S.)* **1952**, *48*, 414−423.
(30) *Standard Methods for the Examination of Water and Wastewater*, 19th ed.; American Public Health Association: Washington, DC, 1995; pp 3.59−3.60.
(31) Ellman, G. L. *Arch. Biochem. Biophys.* **1959**, *82*, 70−77.
(32) Levina, A.; Bailey, A. M.; Champion, G.; Lay, P. A. *J. Am. Chem. Soc.* **2000**, *122*, 6208−6216.
(33) Ellman, G. L.; Lysko, H. *J. Lab. Clin. Med.* **1967**, *70*, 518−527.
(34) Mabbs, F. E.; Machin, D. J. *Magnetism and Transition Metal Complexes*; Chapman and Hall: London, 1973.
(35) Cole, R. B. *J. Mass Spectrom.* **2000**, *35*, 763−772.
(36) Gaskell, S. J. *J. Mass Spectrom.* **1997**, *32*, 677−688.
(37) *IsoPro 3.0*; Senko, M.: Sunnyvale, CA, 1998.
(38) *WinEPR, Version 960801*; Bruker-Franzen Analytic: Bremen, Germany, 1996.
(39) Duling, D. R. *J. Magn. Reson.* **1994**, *B104*, 105−110. The software is available via the Internet at http://epr.niehs.nih.gov/.
(40) (a) Beechem, J. M. *Methods Enzymol.* **1992**, *210*, 37−54. (b) Maeder, M.; Zuberbuhler, A. D. *Anal. Chem.* **1990**, *62*, 2220−2224. (c) Henry, E. R.; Hofrichter, J. *Methods Enzymol.* **1992**, *210*, 129−192.
(41) *Pro-Kineticist, Version 4.10*; Applied Photophysics: Leatherhead, U.K., 1996.
(42) Lay, P. A.; Levina, A. *Inorg. Chem.* **1996**, *35*, 7709−7717.
(43) Levina, A.; Lay, P. A.; Dixon, N. E. *Inorg. Chem.* **2000**, *39*, 385−395.
(44) (a) Rich, A. M.; Armstrong, R. S.; Ellis, P. J.; Freeman, H. C.; Lay, P. A. *Inorg. Chem.* **1998**, *37*, 5743−5753. (b) Rich, A. M.; Armstrong, R. S.; Ellis, P. J.; Lay, P. A. *J. Am. Chem. Soc.* **1998**, *120*, 10827−10836.

a Cr foil as an internal standard (calibration energy, 5989.0 eV, corresponded to the first peak of the first derivative of Cr(0) edge).[45] Averaging, background subtraction, and the calculations of theoretical XAFS spectra were performed using the *XFIT* software package,[45] including *FEFF 4.06*[46] and *FEFF 6.01*[47] algorithms (for SS and MS, respectively), as described previously.[44,48] Conditions, restraints, and constraints applied to the calculations are listed in Table S1 (Supporting Information). The determinancies (N_i/p, where N_i is the number of independent observations and p is the number of varied parameters) of the models used in SS and MS XAFS calculations were estimated by the method of Binsted et al.,[49] taking into account the applied restraints and constraints. Overdetermined models ($N_i/p > 1$) were used in XAFS calculations, which allowed meaningful solutions to be obtained.[49] In all MS XAFS calculations, the values of bond lengths and bond angles within the GSH ligands were restrained to be close (±0.05 Å; ±5°) to those found in the crystal structure of GSH.[50] Release of these restraints led to underdetermined ($N_i/p < 1$) fits and to implausible distortions in the ligand structures. Debye−Waller factors of similar atoms in the ligands were constrained to be equal, thereby decreasing the number of variables in the models. The random errors in the estimated XAFS parameters, arising from the noise in the data, were determined by Monte Carlo analysis within the *XFIT* software.[45] Starting coordinate sets for different models, used for MS XAFS calculations, were obtained using *HyperChem* software.[51]

Reproducibility and Experimental Errors. All the reported results were reproduced in at least two independent experimental series, using different sets of stock solutions and different preparations of Cr(V)−GSH, Cr(V)−GSHOEt, or Cr(III)−GSH. The exception was the XAS of Cr(III)−GSH, where only one preparation was used. Typical relative deviations in the results of parallel experiments were the following: <5% for the analytical methods; <10% for the kinetic studies; and <20% for the EPR spectroscopy and ESMS. The results of XAFS analysis for two different preparations of Cr(V)−GSH agreed within the experimental errors (calculated by Monte Carlo method, see Results).

Results

Electrospray Mass Spectrometry of the Isolated Cr(V)−GSH, Cr(III)−GSH, and Cr(V)−GSHOEt Complexes. Dissolution of Cr(V)−GSH in water results in its rapid decomposition (a dark green color due to the Cr(V) species disappears within ~5 min at [Cr] = 1.0 mM and 22 °C) with the formation of predominantly Cr(III) products (a pale purple solution).[21] Unlike for the Cr(V) 2-hydroxycarboxylato complexes, the Cr(V)−GSH complex is insoluble in polar aprotic solvents, such as DMF or DMSO, where stabilization of Cr(V) is expected.[48,52] Decomposition of the Cr(V)−GSH complex in water was used to detect the signals due to Cr(V) species in ESMS (Figure 1 and Table 1). The only significant difference in the negative-ion ESMS of fresh (~15 s after dissolution, 22 °C) and decomposed (10 min at 22 °C) aqueous solutions of Cr(V)−GSH ([Cr] = 1.0 mM, pH = 8.0, no buffers added) was the presence of a signal with $m/z = -678.5$ (1− species) in the fresh solution (Figure 1). This signal was assigned to a $[Cr^{V}O(LH_3)_2]^-$ species (where the neutral GSH molecule is designated as LH_5) on the basis of the m/z value and the isotopic distribution patterns; experimental and simulated isotopic distributions are given in Figure S1 (Supporting Information).

The negative-ion ESMS of both fresh and decomposed solutions of Cr(V)−GSH (Figure 1; assignment of the signals is given in Table 1) showed the presence of significant amounts of free GSH and GSSG (the signals with $m/z = -306.3$ and -611.5), as well as signals assigned to the Cr(III) products of Cr(V)−GSH decomposition ($m/z = -355.3$, -424.0, -483.6, and -967.4); typical experimental and simulated isotopic distributions for these species are

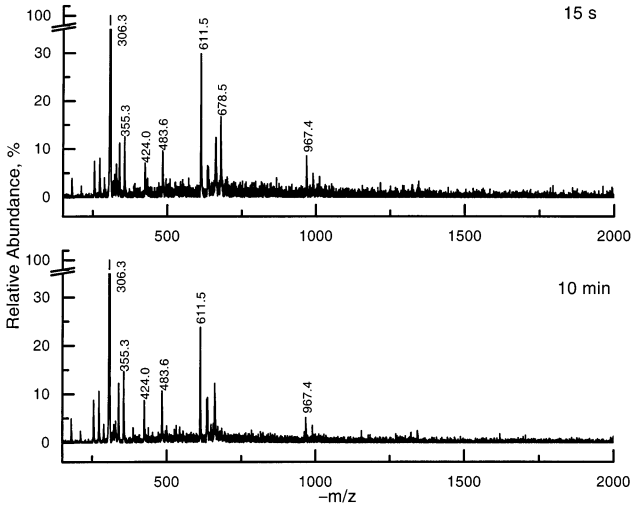

Figure 1. Typical ESMS spectra of aqueous solutions of the isolated Cr(V)−GSH complex ([Cr] = 1.0 mM; pH = 8.0; no buffer added) at 15 s or 10 min after dissolution (22 °C). Assignment of the signals is given in Table 1.

Table 1. Assignment of the Major ESMS Signals[a]

$-m/z$[b]	assignment[c]	$-m/z$[b]	assignment[c]
117.4	$[HCr^{VI}O_4]^-$	483.6	$[Cr^{III}(LLH_4)(LH_4)]^{2-}$
306.3	LH_4^-	611.5	LLH_7^-
334.5	$L'H_3^-$	613.3	$LH_4^-\cdot LH_5$
355.3	$[Cr^{III}(LH)]^-$	635.5	$Na^+\cdot 2LH_4^-$
406.3	$[Cr^{VI}O_3(LH_4)]^-$	668.1	$L'L'H_5^-$
424.0	$[Cr^{III}(LLH_4)(LLH_6)]^{3-}$	669.7	$L'H_3^-\cdot L'H_4$
430.2	$[Cr^{V}O(LH_3)_2(LH_4)_2]^{3-}$	678.5	$[Cr^{V}O(LH_3)_2]^-$
434.6	$[Cr^{VI}O_3(L'H_3)]^-$	734.4	$[Cr^{V}O(L'H_2)_2]^-$
437.5	$Na^+\cdot[Cr^{V}O(LH_3)_3(LH_4)]^{4-}$	967.4	$[Cr^{III}(LLH_5)(LH_4)]^-$
444.9	$2Na^+\cdot[Cr^{V}O(LH_3)_4]^{5-}$	1404.5	$[Cr^{V}O(L'H_3)_4]^-$

[a] Figure 1 and Figures S1−S4, S8, and S11 in Supporting Information. Most of the signals due to the Na^+−ligand adducts, as well as those attributed to impurities in the ligands or ligand fragmentation products formed under the ESMS conditions (Figure S3), are not included. [b] Corresponds to the parent signal in the isotopic distribution (due to ^{52}Cr, ^{12}C, and ^{1}H isotopes, Figure S1). [c] Based on the m/z values and isotopic distribution patterns; typical experimental and simulated isotopic distributions are shown in Figure S1. Designations: LH_5 and LLH_8 are the reduced and oxidized forms of GSH, and $L'H_4$ and $L'L'H_6$ are the reduced and oxidized forms of GSHOEt.

(45) (a) Ellis, P. J.; Freeman, H. C. *J. Synchrotron Radiat.* **1995**, *2*, 190−195. (b) *XFIT for Windows'95*; Australian Synchrotron Research Program: Sydney, Australia, 1996.
(46) Mustre de Leon, J.; Rehr, J. J.; Zabinsky, S. I.; Albers, R. C. *Phys. Rev. B.* **1991**, *44*, 4146−4156.
(47) Rehr, J. J.; Albers, R. C.; Zabinsky, S. I. *Phys. Rev. Lett.* **1992**, *69*, 3397−3400.
(48) Codd, R.; Levina, A.; Zhang, L.; Hambley, T. W.; Lay, P. A. *Inorg. Chem.* **2000**, *39*, 990−997.
(49) Binsted, N.; Strange, R. W.; Hasnain, S. S. *Biochemistry* **1992**, *31*, 12117−12125.
(50) Wright, W. B. *Acta Crystallogr.* **1958**, *11*, 632−642.
(51) *HyperChem, Version 5.1*; Hypercube Inc.: Gainesville, FL, 1996.
(52) Judd, R. J.; Hambley, T. W.; Lay, P. A. *J. Chem. Soc., Dalton Trans.* **1989**, 2205−2210.

given in Figure S1a,b. The presence of Cr(III) species in a fresh solution of Cr(V)−GSH (Figure 1a) is due to a significant decomposition of Cr(V)−GSH during the dissolution process (see the kinetic results that follow). All the mentioned signals due to Cr(III) species, as well as those due to GSH and GSSG, were also detected in the negative-ion ESMS of aqueous solution of the isolated Cr(III)−GSH complex (Figure S2a in Supporting Information).

The unmarked ESMS signals with $-m/z > 306$ (Figure 1) are due to the Na^+ adducts of GSH or GSSG anions. The signals with $-m/z < 306$ (Figure 1) can be attributed either to impurities in GSH or to products of GSH decomposition under the ESMS conditions. All the unmarked signals were also detected in the negative-ion ESMS of GSH Na^+ salt in aqueous solution in the absence of Cr species ($[GS^-] = 5.0$ mM, pH = 7.4, Figure S3a in Supporting Information). Positive-ion ESMS of aqueous solutions of the Cr(V)−GSH and Cr(III)−GSH complexes were dominated by Na^+ adducts of GSH and GSSG; decomposition of Cr(V) did not cause qualitative changes in these spectra (a typical example is shown in Figure S2b). Comparison with the positive-ion ESMS of GSH Na^+ salt (Figure S3b) showed that no significant signals of Cr species were present in the ESMS of the Cr(V)−GSH or Cr(III)−GSH complexes in the positive-ion mode.

A similar rapid decomposition of the Cr(V)−GSHOEt complex was apparent after its dissolution in water as was observed for the Cr(V)−GSH complex; the green color due to the Cr(V) species disappeared within ∼5 min at 22 °C. A comparison of negative-ion ESMS of fresh and decomposed aqueous solutions of Cr(V)−GSHOEt (∼15 s and 10 min at 22 °C, Figure S4 in Supporting Information) revealed the presence of two signals due to unstable species with $m/z = -734.4$ and -1404.5, assigned to $[Cr^VO(L'H_2)_2]^-$ and $[Cr^VO(L'H_3)_4]^-$ (where $L'H_4$ = GSHOEt, Table 1). Other signals detected in the negative-ion ESMS of aqueous solutions of Cr(V)−GSHOEt were those due to the reduced and oxidized forms of GSHOEt, as well as due to a Cr(VI) thioester, $[Cr^{VI}O_3(L'H_3)]^-$ (Figure S4 and Table 1).

Elemental Analyses and TGA of the Cr(V)−GSH Complex. The results of these analyses (Table 2 and Figure S5 in Supporting Information) were consistent with the literature data,[21] except for slightly higher content of Na^+ and volatile components. The results of determination of total sulfur by combustion of the samples were in agreement with the amount of thiolato and disulfide groups, determined with Ellman's reagent (Table 2). Attempts to determine [Cr(V)] in the samples of the Cr(V)−GSH complex by an iodometric titration (a method used for Cr(V) 2-hydroxycarboxylates)[53] were unsuccessful, as no detectable amounts of I_2 were formed in the reactions of Cr(V)−GSH with excess I^- at pH = 0−3.

Magnetic Susceptibility and Solid-State EPR Spectroscopy of the Cr(V)−GSH and Cr(III)−GSH Complexes. The room temperature (295 K) magnetic moment of the Cr(V)−GSH complex ($\mu_{eff} = 2.2 \pm 0.1\ \mu_B$) was consistent with the literature data.[21] This is slightly higher than the spin-only value for a d^1 complex,[34] but close to those observed for well-characterized Cr(V) 2-hydroxycarboxylato complexes, $[Cr^VO(ehba)_2]^-$ (2.05 μ_B)[26] and $[Cr^VO(qa)_2]^-$ (2.10 μ_B).[48]

A sharp asymmetric signal at $g = 1.996$ was observed in the X-band spectrum of the Cr(V)−GSH complex at 22 °C (consistent with the literature data),[21] and a typical anisotropy of an axial system with $S = {}^1/_2$[54] ($g_{||} = 2.005$, $g_\perp = 1.988$) was revealed in the Q-band spectrum (Figure 2). The low-temperature (10 K) X-band EPR spectrum of the solid Cr(III)−GSH complex showed, in addition to the traces of the Cr(V) complex giving rise to a signal at $g = 1.996$, a broad signal with $g \sim 1.98$ and an intense low field signal at $g = 4.5-5.5$ (Figure 3). The last two signals are characteristic of Cr(III) complexes ($S = {}^3/_2$) with a distorted octahedral geometry,[55,56] including Cr(III)−peptide complexes.[57] No such Cr(III) signals were detected in the EPR spectrum of the solid Cr(V)−GSH complex at 10 K (Figure 3). The EPR spectra at 10 K (Figure 3) were acquired on mixtures of solid Cr(V)−GSH or Cr(III)−GSH complexes with BN (mass ratio 1:1), to match the conditions used for XAS measurements. No significant differences in the EPR spectra of the Cr(V)−GSH or Cr(III)−GSH samples before and after XAS measurements were observed, which confirmed the absence of measurable photodamage of the samples during XAS data collection.

X-ray Absorption Spectroscopy of the Cr(V)−GSH and Cr(III)−GSH Complexes. The XANES spectra of the Cr(V)−GSH and Cr(III)−GSH complexes, in comparison with that of a model Cr(V) complex, $Na[Cr^VO(ehba)_2]$

Table 2. Results of Elemental Analyses and TGA of the Cr(V)−GSH Complex[a]

component	% (mass) found[b]	% (mass) calcd[c]	mol/mol Cr
Cr[d]	3.2 ± 0.1	3.17	1.0
Na^+[e]	7.5 ± 0.3	7.15	5.3
C[f]	32.9 ± 0.8	32.21	44.6
H[f]	4.95 ± 0.13	5.21	80.5
N[f]	10.6 ± 0.3	10.50	12.3
S[f]	7.9 ± 0.3	8.01	4.0
S (GSH + GSSG)[g]	8.0 ± 0.3	8.01	4.1
H_2O and/or MeOH[h]	12.2 ± 0.5	12.43	

[a] Typical results of TGA are presented in Figure S5, Supporting Information. [b] Averaged results and standard deviations of 4−6 independent measurements, using two different preparations. [c] For $Na_3[Cr^VO(LH_2)_2] + 1.4NaLH_4 + 0.35Na_2LLH_6 + 3CH_3OH + 6H_2O$. [d] Determined by AAS (in HCl matrix, as Cr(III)) and by UV−vis spectrophotometry (after oxidation to Cr(VI));[29] the results for the two methods agreed within the experimental error. [e] Determined by flame photometry. [f] Determined by combustion of the samples. [g] Determined with Ellman's reagent after reduction of GSSG to GSH with $NaBH_4$.[33] [h] Determined from the mass loss at <160 °C (Figure S5).

(53) Krumpolc, M.; Roček, J. *J. Am. Chem. Soc.* **1977**, *99*, 137−143.

(54) Bencini, A.; Gatteschi, D. In *Inorganic Electronic Structure and Specroscopy*; Solomon, E. I., Lever, A. B. P., Eds.; John Wiley and Sons: New York, 1999; Vol. 1, pp 93−160.

(55) Bonomo, R. P.; Di Bilio, A. J.; Riggi, F. *Chem. Phys.* **1991**, *151*, 323−333.

(56) Weckhuysen, B. M.; Schoonheydt, R. A.; Mabbs, F. E.; Collison, D. *J. Chem. Soc., Faraday Trans.* **1996**, *92*, 2431−2436.

(57) Aisen, P.; Aasa, R.; Redfield, A. G. *J. Biol. Chem.* **1969**, *244*, 4628−4633.

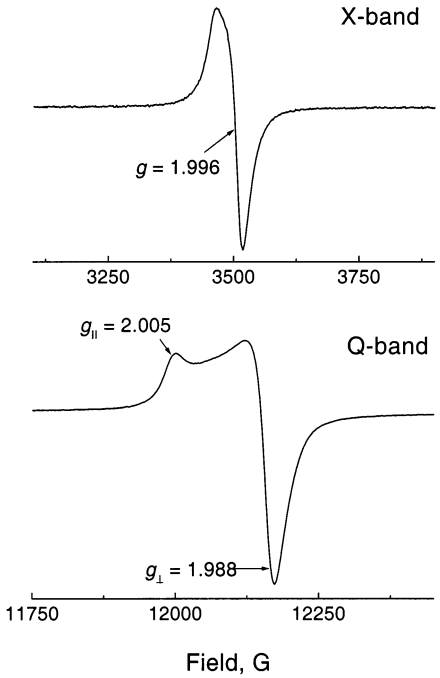

Figure 2. Typical solid-state EPR spectra of the Cr(V)−GSH complex at 22 °C. Microwave frequency, 9.757654 GHz (X-band) or 33.67465 GHz (Q-band); microwave power, 2.0 (X-band) mW or 6.3 mW (Q-band); and modulation amplitude, 1.0 G (X-band) or 5.0 G (Q-band).

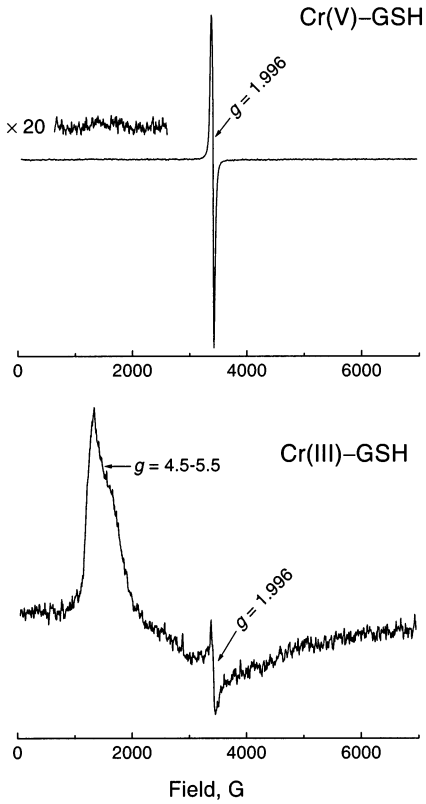

Figure 3. Typical solid-state X-band EPR spectra of the Cr(V)−GSH and Cr(III)−GSH complexes at 10 K (mixtures with BN, mass ratio 1:1). Microwave power 0.20 W; modulation amplitude 2.0 G; microwave frequency 9.463291 GHz (Cr(V)−GSH) or 9.466115 GHz (Cr(III)−GSH).

(characterized by X-ray crystallography[52] and XAS[58]), are shown in Figure 4, and the values of pre-edge and edge absorption energies are given in Table 3. A sharp pre-edge

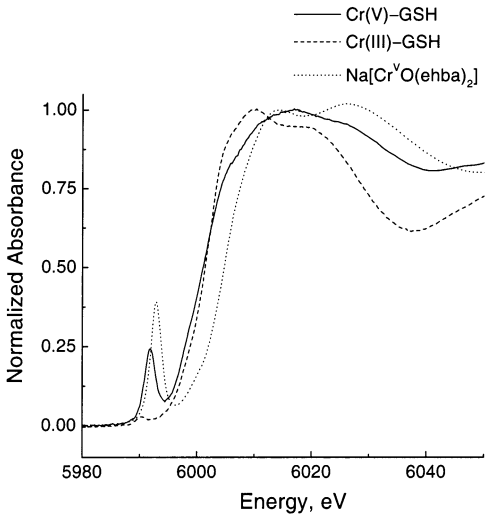

Figure 4. XANES spectra of the Cr(V)−GSH and Cr(III)−GSH complexes in comparison with that of $Na[Cr^{V}O(ehba)_2]$[58] (solids, mixed with BN in 1:1 mass ratio, 10 K).

peak due to a symmetry-forbidden 1s → 3d transition[59,60] in Cr(V)−GSH was close in energy (but lower in intensity) to that of $Na[Cr^{V}O(ehba)_2]$. A weak pre-edge absorbance as well as the edge energy and the general shape of the XANES spectrum for the Cr(III)−GSH complex were typical for octahedral Cr(III) complexes with O and N donors.[59−61] The edge energy for the Cr(V)−GSH complex was close to that of the Cr(III) complex and was significantly lower than that for the well-characterized Cr(V) complex (6004.5 eV).[58]

Single-scattering (SS) XAFS analyses of the first coordination shells were performed to determine the coordination environments in the Cr(V)−GSH and Cr(III)−GSH complexes. The optimized SS XAFS parameters are given in Table 3, the experimental and calculated (corresponding to the best fits, Table 3) XAFS and FT XAFS spectra are shown in Figure S6, and details of SS XAFS analyses are given in Tables S1 and S2, Supporting Information. Criteria for the choice of the best XAFS fits[45,48] included the following: (i) the lowest value of the goodness-of-fit parameter, R (fits with $R < 20\%$ are considered acceptable);[49] (ii) physically reasonable values of the threshold energy, E_0, the scale factor, S_0^2, and the Debye−Waller factors, σ_i^2 (the acceptable ranges of these parameters are given in Table S1);[45] and (iii) the resolution in the bond lengths of two different shells in SS XAFS analysis ($\Delta X \geq 0.11$ Å for $k_{max} = 14$ Å $^{-1}$).[22]

The best SS XAFS fit for the Cr(V)−GSH complex included five donor atoms in three shells: one Cr═O (1.60 Å), two Cr—S (2.30 Å), and two Cr—O/N (2.00 Å) bonds

(58) The XAS of $Na[Cr^{V}O(ehba)_2]$ in the solid state and in aqueous solutions has been studied: (a) Levina, A.; Foran, G. J.; Lay, P. A. *Chem. Commun.* **1999**, 2339−2340. (b) Pattison, D. I.; Levina, A.; Davies, M. J.; Lay, P. A. *Inorg. Chem.*, **2001**, *40*, 214−217. (c) Levina, A.; Lay, P. A.; Codd, R.; Foran, G. J.; Hambley, T. W.; Maschmeyer, T.; Masters, A. F. *Inorg. Chem.*, submitted.

(59) Ellis, P. J.; Joyner, R. W.; Maschmeyer, T.; Masters, A. F.; Niles, D. A.; Smith, A. K. *J. Mol. Catal. A: Chem.* **1996**, *111*, 297−305.

(60) Engemann, C.; Hormes, J.; Longen, A.; Dötz, K. H. *Chem. Phys.* **1998**, *237*, 471−481.

(61) Fainerman-Melnikova, M.; Levina, A.; Weeks, C. L.; Lay, P. A. Unpublished data.

Table 3. Summary of XANES and SS XAFS Data for the Cr(V)−GSH and Cr(III)−GSH Complexes[a]

param[b]	Cr(V)−GSH[c]	Cr(III)−GSH
XANES Spectra		
edge energy, eV[d]	6001.2	6001.5
pre-edge energy, eV	5991.8	5990.4
pre-edge intensity, %[e]	23.7	2.8
SS XAFS Analysis[f]		
N_i/p	1.5	2.0
R, %	10.7	8.3
$-\Delta E_0$, eV	5.0	5.1
S_0^2	0.90	0.90
shell 1	Cr═O	Cr−O/N
N	0.92 ± 0.16	2.78 ± 0.20
X, Å	1.60	1.93
σ^2, Å^2	0.0062	0.00075
shell 2	Cr−S	Cr−O/N
N	1.79 ± 0.15	3.10 ± 0.25
X, Å	2.30	2.05
σ^2, Å^2	0.0016	0.0025
shell 3	Cr−O/N	
N	2.20 ± 0.12	
X, Å	2.00	
σ^2, Å^2	0.00093	

[a] Details of the SS XAFS calculations are given in Tables S1 and S2 and Figure S6, Supporting Information. [b] Designations: N_i/p is the determinancy of the model (N_i = number of independent observations, p = number of varied parameters), calculated taking into account the applied restraints and constraints;[49] R is the goodness-of-fit parameter; $\Delta E_0 = E_0 - 6005$ (eV), where E_0 is the threshold energy; S_0^2 is the scale factor; N is the number of scatterers; X (Å) is the absorber−scatterer distance; and σ^2 (Å^2) are the Debye−Waller factors. Errors in the optimized parameters (arising from the noise in experimental data; calculated by Monte Carlo method)[45] were <0.5 eV for ΔE_0, <0.05 for S_0^2, <0.0003 Å^2 for σ^2, and <0.007 Å for the X values. [c] Two independent preparations of Cr(V)−GSH were used; the results for the both agreed within the experimental errors. [d] Determined at 50% of the edge jump (Figure 4). [e] Peak height relative to the normalized edge jump (Figure 4). [f] Results for the best SS XAFS fits; see text and Table S2 (Supporting Information) for the results of application of various SS XAFS models.

(R = 10.7%, Table 3, numbers of scatterers in each shell were allowed to vary during the optimization). Removal of any of these shells led to poor fits (R = 25−68%, columns 1−4 in Table S2). The Cr−O/N and Cr−S shells were clearly resolved in the FT XAFS spectrum of the Cr(V)−GSH complex (Figures 5 and S6). Five- or six-coordinate structures have been observed for Cr(V) oxo complexes.[7,19,62] The SS XAFS fits with fixed numbers of scatterers in each shell confirmed the preference of a five-coordinate model (1Cr═O + 2Cr−S + 2Cr−O/N, R = 11.7%) over six-coordinate models (1Cr═O + 2 Cr−S + 3Cr−O/N, R = 14.8−15.3%) for Cr(V)−GSH (columns 5−7 in Table S2).

The best SS XAFS fit for the Cr(III)−GSH complex (Table 3) corresponded to a six-coordinate structure with three short (1.93 Å) and three long (2.05 Å) Cr−O/N bonds. The SS XAFS analysis unambiguously showed the absence of Cr−S bonds in the Cr(III)−GSH complex (Table S2), in agreement with the absence of a Cr−S shell in the corresponding FT XAFS spectrum (Figure S6). No attempts were made to perform a structural modeling of a Cr(III)−GSH complex using MS XAFS, as the formation of at least four different Cr(III) species has been detected by ESMS (Figures 1 and S2).

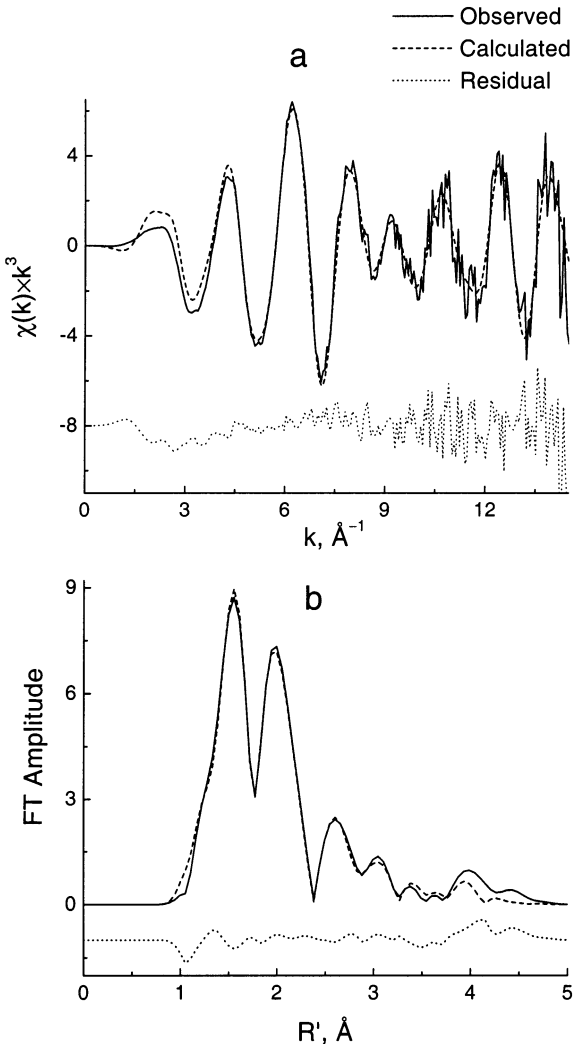

Figure 5. Experimental (solid, 10 K) and calculated (MS, from model 4 in Chart 1) XAFS spectra (a) and their Fourier transforms (b) for the Cr(V)−GSH complex. Window functions applied to the Fourier transforms are shown in Figure S7.

Proposed five-coordinate structures of the isolated Cr(V)−GSH complex (including the atoms of the first four coordination shells, models 1−4 in Chart 1), used to initiate MS XAFS calculations, were in agreement with the following: (i) the structure of the first coordination shell determined by SS XAFS analysis (Tables 3 and S2); (ii) the assignment of the Cr(V) species as $[Cr^{V}O(LH_3)_2]^-$ from the ESMS data (Figure 1 and Table 1); (iii) the EPR spectroscopic[16,63] and ESMS[64] studies of Cr(V) complexes with model thiols, which showed that the Cr is likely to be bound to thiolato and deprotonated amido donors in the Cr(V)−GSH complex; and (iv) the possibility of distorted trigonal bipyramidal or square pyramidal geometries for five-coordinate Cr(V) oxo complexes.[62] Possible geometric isomers of a trigonal bipyramidal structure[48,62,65] are presented by models 1−3 in Chart 1. A square pyramidal isomer (model 4) had the amido donors in *trans* positions; a similar model with the amido donors in *cis* positions was rejected from the steric considerations

(62) Farrell, R. P.; Lay, P. A. *Comments Inorg. Chem.* **1992**, *13*, 133−175 and references therein.

(63) Zhang, L.; Levina, A.; Lay, P. A. To be submitted.
(64) Levina, A.; Zhang, L.; Lay, P. A. To be submitted.
(65) Codd, R.; Lay, P. A. *J. Am. Chem. Soc.* **1999**, *121*, 7864−7876.

Table 4. Summary of Results of MS XAFS Modelling for the Cr(V)−GSH Complex[a]

	model no.[c]					
param[b]	1	2	3	4	5	6
N_i/p	1.04	1.04	1.04	1.04	1.03	1.03
R, %	14.3	10.8	12.2	10.6	11.2	11.9
$-\Delta E_0$, eV	5.1	5.8	4.3	5.5	4.8	5.4
S_0^2	0.98	0.95	0.97	0.96	0.82	0.82
Cr═O(1), Å	1.61	1.61	1.62	1.61	1.62	1.62
Cr−S(2,4), Å [d]	2.30	2.30	2.31	2.31	2.31	2.31
Cr−N(3,5), Å [d]	2.00	1.99	1.98	1.99	2.00	2.02
Cr−O(22), Å					2.01	
Cr−N(18), Å						1.95
σ^2 O(1), Å^2	0.0073	0.0082	0.012	0.0079	0.0057	0.0062
σ^2 S(2,4), Å^2	0.0033	0.0038	0.0068	0.0035	0.0023	0.0006
σ^2 N(3,5), Å^2	0.0008	0.0015	0.0005	0.0011	0.0013	0.0005
σ^2 O(22), Å^2					0.0048	
σ^2 N(18), Å^2						0.0005

[a] Details of MS XAFS calculations are given in Figure S7 and Tables S1 and S3−S5, Supporting Information. [b] Designations of the parameters correspond to Table 3; numbering of the atoms corresponds to Chart 1. Random errors in the bond lengths (calculated by Monte Carlo method)[45] were <0.008 Å; expected systematic errors are 0.01−0.02 Å.[44] [c] Designations of the models correspond to Chart 1. [d] The optimized bond lengths in the both GSH ligands agreed within 0.01 Å.

(using molecular models built with *HyperChem* software).[51] Models 5 and 6 (Chart 1) represent two of the possible six-coordinate structures of the Cr(V)−GSH complex, with either an aqua ligand or the amido group of the Gly residue in GSH as the sixth ligand. Numbers of scatterers, included in models 1−6, were chosen by the following criteria: (i) all the atoms that are likely to be found within 5 Å of the Cr absorber[44] were included (the absorber−scatterer distances for the optimized model are shown in Table S3, Supporting Information); and (ii) inclusion of additional scatterers would lead to underdetermined fits[49] (the N_i/p values for the applied models are given in Table 4).

The results of MS XAFS calculations for the Cr(V)−GSH complex, starting from different models, are listed in Table 4, the experimental and calculated (from model 4) XAFS and FT XAFS spectra are shown in Figure 5, and the corresponding optimized structure of the Cr(V)−GSH complex is shown in Figure 6. Further details of the MS XAFS calculations are given in the Supporting Information: the applied window functions are shown in Figure S7; the applied conditions, restraints, and constraints are listed in Table S1; the most significant scattering paths (2−5 legs) for the optimized model are given in Table S3; the Debye−Waller factors for the atoms of second and further coordination shells are listed in Table S4; and optimized bond angles around the Cr atom are given in Table S5. The last two tables include the results of MS XAFS calculations based on models 1−6 (Chart 1). For all the models, the optimized values of bond lengths and angles in the ligands were within 0.02 Å and 2°, respectively, of the restrained values (Table S1).

Application of the five-coordinate models 1−4 to the MS XAFS calculations for the Cr(V)−GSH complex led to excellent goodness-of-fit values (R = 10.6−14.3%, Table 4 and Figure 5).[45,49] The optimized values of the Cr−ligand distances were the same for models 1−4, within experimental error (Table 4); these values agreed well with the values

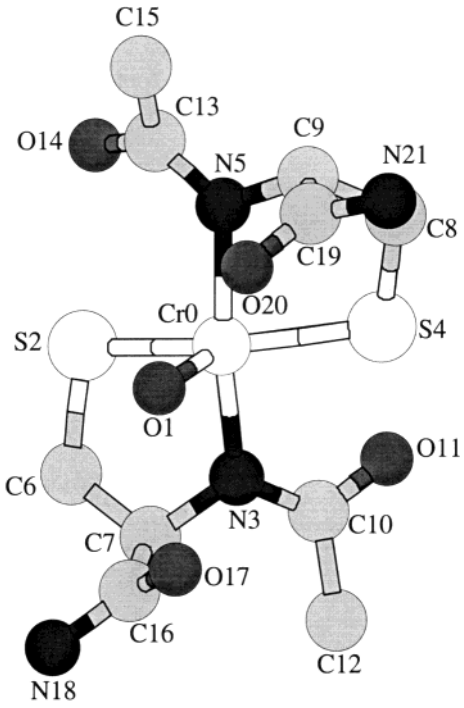

Figure 6. Structure of the Cr(V)−GSH complex (solid, 10 K), optimized by MS XAFS calculations (corresponds to model 4 in Tables 4, S4, and S5).

determined by SS XAFS calculations (Table 3). Calculations started from models 2 or 4 (Chart 1) led to the lowest and close R values (Table 4), and to similar geometries of the optimized models (distorted trigonal bipyramids with the less bulky amido N donors in axial positions, Figure 6 and Table S5). All the optimized σ_i^2 values for models 2 and 4 were within a physically reasonable range (0.0010−0.010 Å^2, Tables 4 and S4).[44,45] The optimized σ_i^2 values of the oxo group for models 2 and 4 (∼0.008 Å^2, Table 4) were higher than those usually observed for the scatterers in the first coordination shells (0.001−0.004 Å^2),[44,45] but close to those observed for the oxo group in the Cr(V) quinato complex.[48] Such relatively high σ_i^2 values point to a significant disorder in the position of the oxo group.[48] Application of other geometric isomers of the trigonal bipyramidal structure (with two S donors, or one S and one N donor, in axial positions; models 1 and 3 in Chart 1, respectively) led to a significant deterioration of the fits: (i) the R values were significantly higher compared with those for models 2 and 4 (Table 4); (ii) the σ_i^2 values for the atoms C6 and C8 in the second coordination shell were unreasonably high (0.02 Å^2, Table S4); and (iii) for model 3, the σ_i^2 values for the amido donors were unreasonably low (0.0005 Å^2, Table 4). Thus, the MS XAFS calculations for Cr(V)−GSH, using different five-coordinate models, showed a significant preference toward a trigonal bipyramidal model with amido donors in axial positions, which enables the most sterically demanding thiolato and oxo donors to be as far away as possible (Chart 1 and Figure 6).

According to the MS XAFS results for models 1−4, the best six-coordinate models for the Cr(V)−GSH complex (models 5 and 6 in Chart 1) had the amido donors in *trans*

Chart 1. Models Used To Initiate the MS XAFS Calculations for the Cr(V)−GSH Complex

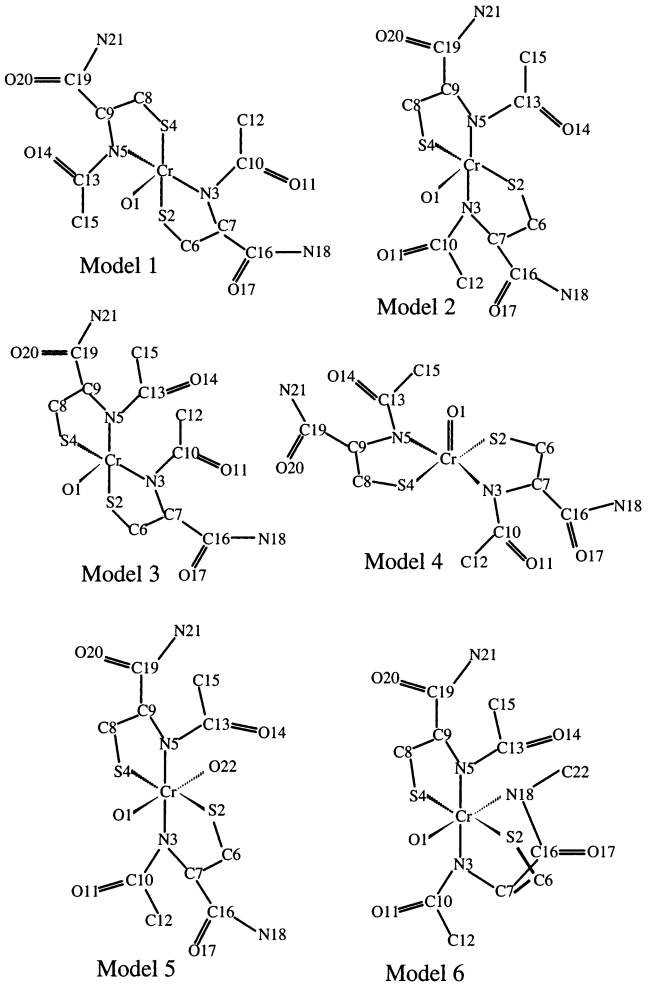

positions. The optimized *R* values for these models were significantly higher compared to the best five-coordinate models (Table 4). The values of the scale factor (S_0^2) for the six-coordinate models (Table 4) were lower than those usually observed in MS XAFS calculations (∼0.9),[44,45,48] which points to the absence of the sixth scatterer in the first coordination shell of Cr.[45] In addition, some of the optimized σ_i^2 values for models 5 and 6 were unreasonably high or low (Tables 4 and S4). Thus, the results of MS XAFS calculations, in agreement with those of SS XAFS (Table S2), point to a preference of five-coordinate models over six-coordinate ones for the Cr(V)−GSH complex.

Kinetics and Products of Cr(V)−GSH Decomposition in Aqueous Solutions. The X-band EPR spectra of Cr(V)−GSH in aqueous solutions (Figure 7, [Cr] = 1.0 mM, pH = 8.0, no buffers added, 22 °C) possessed a main signal with g_{iso} = 1.9960 (LW = 3.5 × 10^{-4} cm^{-1}) and minor signals with g_{iso} = 1.9857, 19825, 1.9770, and 1.9725 (LW = (0.6−2.2) × 10^{-4} cm^{-1}), in agreement with the literature data for the solutions of the Cr(V)−GSH complex, as well as for the Cr(VI) + GSH systems.[11−13,20,21] All the signals disappeared within ∼10 min (22 °C), but the relative intensities of the signals with g_{iso} = 1.9857 and 1.9725 increased during the course of Cr(V)−GSH decomposition (Figure 7).

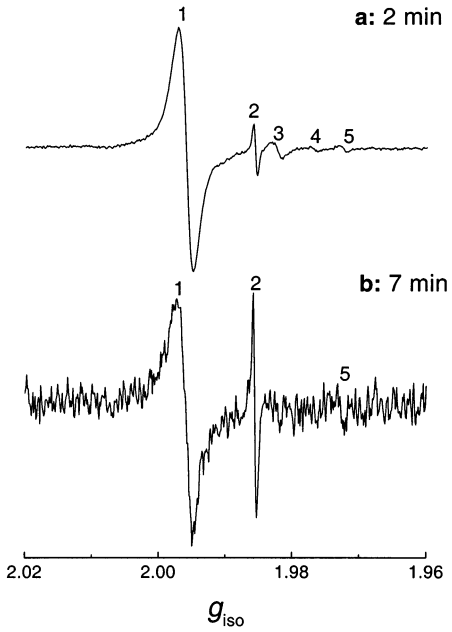

Figure 7. Typical X-band EPR spectra of the Cr(V)−GSH complex after dissolution in aqueous solutions. Conditions: [Cr] = 1.0 mM, pH = 8.0, 22 °C; time after dissolution 2 min (a) or 7 min (b). Spectrometer settings: microwave frequency, ∼9.67 GHz; microwave power, 2.0 mW; modulation amplitude, 1.0 G, and receiver gain, 10^4. The g_{iso} values for the designated signals are the following: 1.9960 (1), 1.9857 (2), 1.9825 (3), 1.9770 (4), and 1.9725 (5).

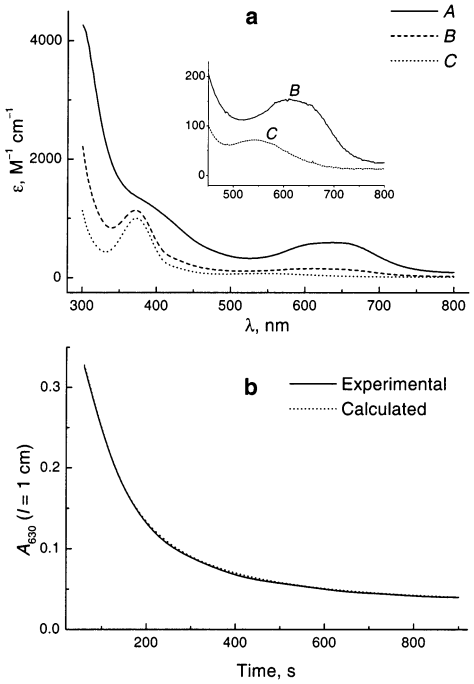

Figure 8. Typical results of global kinetic analysis for the decomposition of the Cr(V)−GSH complex in aqueous solution: ([Cr] = 1.0 mM, pH = 8.0, no buffers added, 22 °C); (a) estimated spectra of the reacting species (kinetic scheme **A** → **B** → **C**, observed rate constants 1.4 × 10^{-2} s^{-1} and 3.9 × 10^{-3} s^{-1}); (b) experimental and calculated kinetic curves at 630 nm.

Time-dependent UV−vis spectroscopy (Figure 8a; conditions as already described) revealed biphasic kinetics for the decomposition of the Cr(V)−GSH complex in aqueous solutions, which were best fitted by a sequence of two pseudo-first-order steps (Figure 8b). The estimated spectrum of the initial compound (**A** in Figure 8a, λ_{max} = 638 nm,

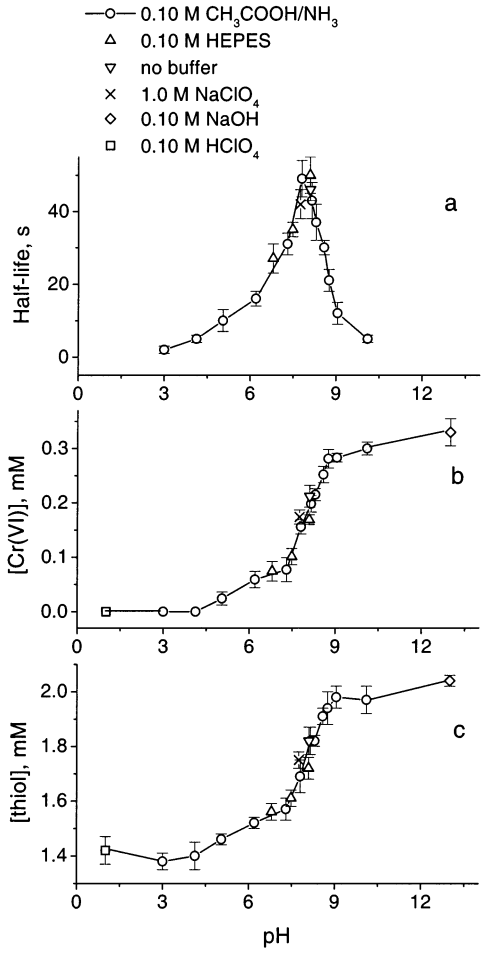

Figure 9. Results of decomposition studies for the Cr(V)−GSH complex (1.0 mM Cr) in aqueous solutions at 25 °C (averaged results and standard deviations of three independent measurements are shown): (a) half-life times ($\tau_{1/2}$), determined from the absorbance changes at 630 nm; (b) values of [Cr(VI)] in the reaction products, determined with diphenylcarbazide;[30] and (c) values of [GSH] in the reaction products, determined with Ellman's reagent.[31] Measurements of (b) and (c) were performed at $\tau = 10\tau_{1/2}$.

$\epsilon_{max} = 5.9 \times 10^2$ M^{-1} cm^{-1}) was similar to the literature spectrum for the Cr(V)−GSH complex but the significantly higher value of ϵ_{max} (1.0×10^3 M^{-1} cm^{-1} at 650 nm), reported previously,[21] was probably due to an extrapolation error, using kinetic data at a single wavelength. The spectrum of the decomposition product (**C** in Figure 8a) possessed the characteristic absorbance of $[Cr^{VI}O_4]^{2-}$ ($\lambda_{max} = 372$ nm),[66] as well as a weak d−d transition band typical for octahedral Cr(III) species with O and N donors ($\lambda_{max} = 543$ nm, $\epsilon_{max} = 72$ M^{-1} cm^{-1}).[67] The estimated spectrum of the intermediate (**B** in Figure 8a) was distinguished from that of product **C** with the absorbance band at $\lambda_{max} = 612$ nm ($\epsilon_{max} = 154$ M^{-1} cm^{-1}), which can be attributed to secondary Cr(V) species ($g_{iso} = 1.9857$ and 1.9725, signals 2 and 5 in Figure 7), and/or to Cr(IV)−GSH species.

The pH- and buffer-dependencies of the decomposition of the Cr(V)−GSH complex are summarized in Figure 9. The stability−pH dependence was bell-shaped, with maximal half-life times of the Cr(V) complex (40−50 s at [Cr] = 1.0 mM and 25 °C, determined from the decrease of absorbance at 630 nm) observed at pH = 7.5−8.0 (Figure 9a). This was independent of the presence and nature of the buffer (0.10 M CH_3COOH/NH_3 or HEPES) and the ionic strength (0−1.0 M $NaClO_4$).

Decomposition of Cr(V) complexes in aqueous solutions proceeds through parallel disproportionation (eq 1, favored in neutral and basic media) and ligand oxidation (eq 2, favored in acidic media); the ratio between the two pathways can be determined from the concentration of Cr(VI) in the reaction products:[68,69]

$$3Cr(V) \rightarrow 2Cr(VI) + Cr(III) \quad (1)$$

$$Cr(V)-(lig)_n \rightarrow Cr(III) + \text{oxidized lig} \quad (2)$$

The results of Cr(VI) determination in the decomposition products of Cr(V)−GSH at different pH values (Figure 9b) showed that practically all Cr(V) decomposed by ligand oxidation (eq 2) at pH < 5, 5−20% of Cr(V) decomposed by disproportionation (eq 1) in neutral media (pH = 6−8), and even at strongly basic conditions (pH = 13), only ∼50% of Cr(V) decomposed by disproportionation. The results of the [Cr(VI)] determination were not affected by the presence of free GSH (shown by additions of 0.20−3.0 mM of Cr(VI) to the analyzed solutions), as the Cr(VI) + GSH reactions at pH = 1−13 were negligibly slow compared with the Cr(V) decomposition at the same pH values. The results in Figure 9a,b are in marked contrast with those for the decomposition of Cr(V) 2-hydroxycarboxylates, where disproportionation (eq 1) is the dominant mechanism at pH ≥ 2, and maximal stability of Cr(V) is observed at pH = 3−4.[48,68]

Contrary to the results of O'Brien et al.,[21] ≥1.4 mol of thiol groups per mol of Cr were detected (using Ellman's reagent) in fresh Ar-saturated solutions of the decomposition products of the Cr(V)−GSH complex. The failure in the previous work[21] to detect thiol groups was probably due to the use of aged, air-saturated solutions, where GSH was oxidized to GSSG.[70] A comparison of the values of [Cr(VI)] and [thiol] (Figure 9b,c) showed that the formation of 1.0 mol of Cr(VI) corresponded to the release of 2.0 ± 0.1 mol of GSH during the decomposition of the Cr(V)−GSH complex. Time-dependent determinations of [thiol] showed, in agreement with the XAFS data (Tables 3 and S2), that no significant amounts of Cr(III)−S(thiolato) bonds were formed during the decomposition of Cr(V)−GSH at pH = 1−13 (these bonds can be determined from their slow reactions with Ellman's reagent).[32] Decomposition studies of the Cr(V)−GSH complex (1.0 mM) in the presence of added GSH (1.0−5.0 mM) showed that no significant reactions of Cr(V) with the added GSH occurred at pH = 1−13

(66) Brasch, N. E.; Buckingham, D. A.; Evans, A. B.; Clark, C. R. *J. Am. Chem. Soc.* **1996**, *118*, 7969−7980.
(67) Larkworthy, L. F.; Nolan, K. B.; O'Brien, P. In *Comprehensive Coordination Chemistry*; Wilkinson, G., Gillard, R. D., McCleverty, J. A., Eds.; Pergamon Press: Oxford, U.K., 1987; Vol. 3, pp 699−969 and references therein.
(68) Krumpolc, M.; Roček, J. *Inorg. Chem.* **1985**, *24*, 617−621.
(69) Equation 1 presents the stoichiometry of a multistep reaction (detailed mechanistic studies have been recently published).[43]
(70) Scarpa, M.; Momo, F.; Viglino, P.; Vianello, F.; Rigo, A. *Biophys. Chem.* **1996**, *60*, 53−61.

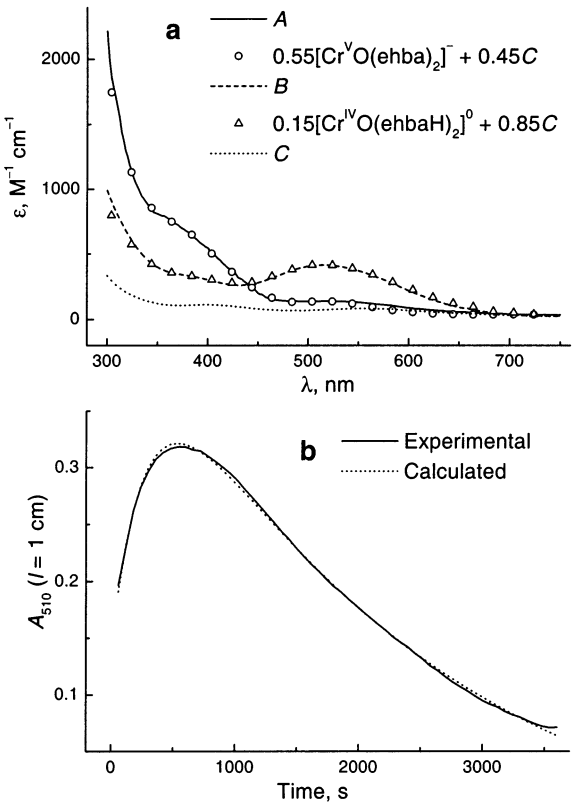

Figure 10. Typical results of global kinetic analysis for the reaction of the Cr(V)−GSH complex with ehbaH_2/ehbaH buffer ([Cr] = 1.0 mM, [ehba] = 0.20 M, pH = 3.5, 22 °C): (a) estimated spectra of the reacting species and comparison with the known spectra of Cr(V/IV)−ehba complexes[43,72] (kinetic scheme **A** → **B** → **C**, observed rate constants 3.6 × 10^{-3} s^{-1} and 4.0 × 10^{-4} s^{-1}); (b) experimental and calculated kinetic curves at 510 nm.

(determined from the values of [thiol] in solutions after decomposition of Cr(V)). The analytical data (Table 2 and Figure 9b,c) led to the following averaged composition of the solid Cr(V)−GSH (in molar equivalents): $1.0Na_3[Cr^VO(LH_2)_2] + 1.4NaLH_4 + 0.35Na_2LLH_6 + 3CH_3OH + 6H_2O$ (where LH_5 = GSH and LLH_8 = GSSG).

Reaction of the Cr(V)−GSH Complex with 2-Ethyl-2-hydroxybutanoate (ehba). Relatively stable Cr(V)− and Cr(IV)−ehba complexes are widely used as models in the studies of Cr(V) and Cr(IV) reactions with biomolecules;[7,25,28,32] UV−vis spectra of these complexes are well-known.[43] Therefore, time-dependent UV−vis spectroscopy was used in the studies of the reaction of ehbaH_2/ehbaH (0.20 M; pH = 3.5; 22 °C) with the Cr(V)−GSH complex ([Cr] = 1.0 mM), to provide information on the composition of the Cr(V)−GSH complex; typical results are shown in Figure 10. The kinetic data were fitted with a sequence of two pseudo-first-order steps (typical observed and calculated kinetic curves are shown in Figure 10b). The calculated spectrum of the initial compound, **A** (Figure 10a), possessed shoulders at 350 and 510 nm, characteristic for $[Cr^VO(ehba)_2]^-$.[26,43] No absorbance at ∼630 nm, characteristic for the Cr(V)−GSH complex (**A** in Figure 8a), was observed in the presence of excess ehba (**A** in Figure 10a). A comparison with the spectrum of pure $[Cr^VO(ehba)_2]^-$ (Figure 10a)[43] revealed that **A** consists of $[Cr^VO(ehba)_2]^-$ (55 mol %) and a Cr(III) product **C** (45 mol %). This was confirmed by the X-band EPR spectrum of the solution of Cr(V)−GSH in ehbaH_2/ehbaH buffer ([Cr] = 1.0 mM; [ehba] = 0.20 M; pH = 3.5; reaction time 2−3 min at 22 °C), which consisted of a sharp signal due to $[Cr^VO(ehba)_2]^-$ (g_{iso} = 1.9783, $A_{iso}(^{53}Cr) = 17.1 \times 10^{-4}$ cm^{-1}, LW = 1.0×10^{-4} cm^{-1}),[26] and a broad signal of Cr(III) species ($g_{iso} \sim 1.98$, LW ∼ 2×10^{-2} cm^{-1}).[55,56] Thus, dissolution of Cr(V)−GSH in the ehbaH_2/ehbaH buffer (0.20 M; pH 3.5) was accompanied by two parallel fast (time scale < 1 min; Figure 10) processes: ligand-exchange reaction of Cr(V)−GSH with ehba, and reduction of Cr(V) to Cr(III). At a longer time scale (1−10 min, Figure 10b), an increase of absorbance with λ_{max} = 510 nm was observed, corresponding to the formation of $[Cr^{IV}O(ehbaH)_2]^0$.[58a,71] The estimated spectrum of intermediate **B** (Figure 10a) consisted of those due to $[Cr^{IV}O(ehbaH)_2]^0$ (15 mol %) and due to the Cr(III) species **C** (85 mol %). This intermediate then slowly decayed with the formation of Cr(III) species **C** (time scale > 1 h at 22 °C; Figure 10). Thus, the observed changes in UV−vis spectra during the reaction of the Cr(V)−GSH complex with ehbaH_2/ehbaH (Figure 10) correspond to a relatively slow reduction of $[Cr^VO(ehba)_2]^-$ (which is formed in the initial fast ligand-exchange reaction) by GSH with the formation of Cr(IV)−ehba intermediates and Cr(III) products.[28,72]

Intermediates and Products of the Cr(VI) + GSH Reaction (High Reagent Concentrations). The Cr(VI) + GSH reaction under the conditions used for the isolation of the Cr(V)−GSH complex ($[Cr(VI)]_0$ = 50 mM, $[GSH]_0$ = 0.50 M, pH = 7.0, adjusted with NaOH, 0 °C)[21] was studied by ESMS and UV−vis and EPR spectroscopies, to provide additional information on the nature of Cr(V)−GSH species. This reaction was accompanied by distinct color changes: in the first ∼15 s, an orange color developed, which changed to dark green within ∼1 min and to purple after ∼1 h. Typical UV−vis spectra of the orange, green, and purple solutions (diluted 100-fold with H_2O) are shown in Figure 11, and the corresponding ESMS results are presented in Figure S8, Supporting Information (assignment of the species is given in Table 1).

The orange color is due to the mixture of chromate $[Cr^{VI}O_4]^{2-}$ (m/z = −117.4 for the protonated form, λ_{max} = 372 nm)[66] and the Cr(VI) thioester $[Cr^{VI}O_3(LH_4)]^-$ (m/z = −406.3, λ_{max} = 430 nm).[73] The corresponding thioester has also been observed for GSHOEt (Table 1). To our knowledge, this is the first observation of Cr(VI) thioesters by mass spectrometry, although the existence of these species in aqueous solutions of Cr(VI) and biological thiols has been suggested from UV−vis, NMR, and Raman spectroscopies.[9,10,73−76]

(71) Codd, R.; Lay, P. A.; Levina, A. *Inorg. Chem.* **1997**, *36*, 5440−5448.
(72) Ghosh, S. K.; Bose, R. N.; Gould, E. S. *Inorg. Chem.* **1987**, *26*, 3722−3727.
(73) McAuley, A.; Olatunji, M. A. *Can. J. Chem.* **1977**, *55*, 3335−3340.
(74) Brauer, S. L.; Wetterhahn, K. E. *J. Am. Chem. Soc.* **1991**, *113*, 3001−3007.
(75) Brauer, S. L.; Hneihen, A. S.; McBride, J. S.; Wetterhahn, K. E. *Inorg. Chem.* **1996**, *35*, 373−381.
(76) Meloni, P. A.; Czernuszewicz, R. S. *Vib. Spectrosc.* **1993**, *5*, 205−213.

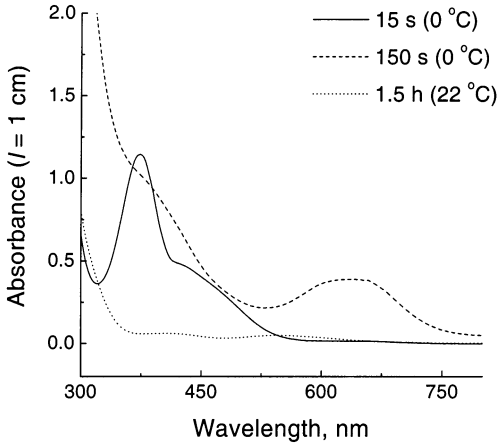

Figure 11. Typical UV−vis spectra of the reaction mixtures (diluted 100-fold with H_2O; ∼30 s after the dilution; 22 °C) for the reactions of 50 mM Cr(VI) with 0.50 M GSH at pH 7.0 (adjusted with NaOH).

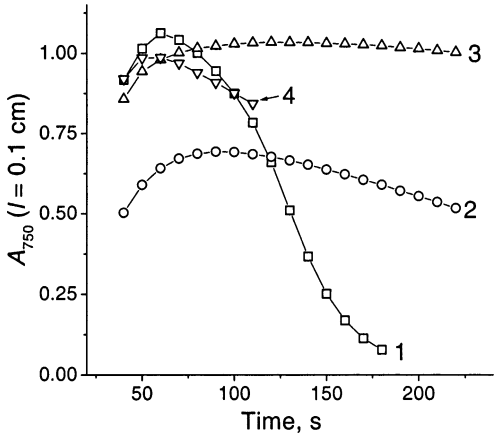

Figure 12. Typical kinetic curves at 750 nm for the formation and decomposition of the green intermediate during the reactions of Cr(VI) (50 mM) with GSH at pH 7.0 (adjusted with NaOH). Conditions: $[GSH]_0$ = 0.50 M, 25 °C (1); $[GSH]_0$ = 0.30 M, 25 °C (2); $[GSH]_0$ = 0.50 M, 5 °C (3); and $[GSH]_0$ = 0.90 M, 5 °C (4).

The green color (λ_{max} = 630 nm) corresponded to nearly complete (∼90%) disappearance of the Cr(VI) signals in ESMS and to the appearance of several new signals (Figure S8; the abundance of the signal due to GS^-, $m/z = -306.3$, is taken as a 100% reference): (i) $m/z = -678.5$ (0.9%), which was previously observed in fresh aqueous solutions of Cr(V)−GSH (Figure 1) and was assigned to $[Cr^VO(LH_3)_2]^-$; and (ii) $m/z = -430.2$, −437.5, and −444.9 (1.4%, 0.8% and 0.5%, respectively). The latter three signals were due to 3− species (determined from isotopic distribution patterns) and were assigned to $[Cr^VO(LH_3)_2(LH_4)_2]^{3-}$, $\{Na^+\cdot[Cr^VO(LH_3)_3(LH_4)]^{4-}\}^{3-}$, and $\{2Na^+\cdot[Cr^VO(LH_3)_4]^{5-}\}^{3-}$ species (Table 1).

The purple color corresponded to a typical UV−vis spectrum of Cr(III) species with O and N donors (λ_{max} = 410 and 550 nm, Figure 11)[67] and to the appearance of ESMS signals with $m/z = -424.0$ and −483.6 (Figure S8), which were assigned to Cr(III) complexes of GSH and GSSG (Table 1). The same signals of Cr(III) species were observed in decomposed aqueous solutions of Cr(V)−GSH, as well as for the isolated Cr(III)−GSH complexes (Figures 1 and S2). No signals of the Cr(V) or Cr(VI) species were observed in the ESMS of the purple solution (Figure S8).

A typical X-band EPR spectrum (22 °C) of the reaction mixture (Figure S9a, $[Cr(VI)]_0$ = 50 mM, $[GSH]_0$ = 0.50 M, pH = 7.0, reaction time ∼2 min at 22 °C) possessed a main signal with g_{iso} = 1.9958 (LW = 4.2×10^{-4} cm^{-1}) and two minor signals with g_{iso} = 1.9857 (LW = 0.6×10^{-4} cm^{-1}) and g_{iso} = 1.9825 (LW = 2.5×10^{-4} cm^{-1}). All three EPR signals disappeared simultaneously over ∼40 min at 22 °C, which corresponded to the change in solution color from green to purple. Dilution of the reaction mixture 100-fold with H_2O (Figure S9b; reaction time in concentrated solution 2 min; time after dilution 2 min; 22 °C) led to a slight shift in the g_{iso} value (1.9960) and to a decrease in the line width (3.3×10^{-4} cm^{-1}) for the main signal. In addition, the relative intensity of the signal with g_{iso} = 1.9857 increased significantly, and new weak signals with g_{iso} = 1.9770 and 1.9725 appeared (Figure S9b). The resultant EPR spectrum was very similar to that for the aqueous solution of the isolated Cr(V)−GSH complex (Figure 7a). As for the latter system (Figure 7b), the Cr(V) EPR signals in the diluted reaction mixture persisted for ∼10 min (22 °C), and the relative intensities of the signals with g_{iso} = 1.9857 and 1.9725 increased during the course of decomposition of the Cr(V) complex.

Kinetics of the formation and decomposition of the green intermediate were further studied in undiluted solutions ($[Cr(VI)]_0$ = 10−70 mM, $[GSH]_0$ = 0.10−0.90 M, pH 7.0, 5 or 25 °C). Because of the high intensity of the color, the absorbance was measured at 750 nm (specific for the green intermediate, Figure 11) in a short path length cell (0.10 cm). Typical kinetic curves are shown in Figure 12. The value of $\epsilon_{max} = (2.0 \pm 0.1) \times 10^2$ M^{-1} cm^{-1} was temperature-independent and did not change at $[Cr(VI)]_0 \geq 30$ mM and $[GSH]_0 \geq 0.40$ M. The kinetic data (Figure 12) strongly indicate that the conditions of O'Brien et al.[21] (50 mM Cr(VI), 0.50 M GSH, pH 7.0, 150 s at 0 °C) led to quantitative formation of Cr(V) species (≥95% of total Cr).

Intermediates and Products of the Cr(VI) + GSH Reaction (Low Reagent Concentrations). Kinetics of the Cr(VI) + GSH reaction were also studied under the conditions used by Gaggelli et al.[24] to characterize the purported $Cr(V)_2GSH_2$ species ($[Cr(VI)]_0$ = 5.0 mM, $[GSH]_0$ = 20.0 mM, $[GSSG]_0$ = 5.0 mM, pH = 7.4, adjusted with NaOH, in D_2O solution, 22 °C). Time-dependent UV−vis spectra of the reaction mixtures (Figure 13) possessed the following features: (i) a strong absorbance with λ_{max} = 372 nm due to $[Cr^{VI}O_4]^{2-}$ [66] decayed over >2 h; (ii) a shoulder at 400−500 nm due to $[Cr^{VI}O_3(LH_4)]^-$ [9,10,73] was observed during the first ∼20 min of reaction; (iii) a weak absorbance at 600−700 nm, probably due to Cr(V)−GSH species, was observed at 3−20 min, and its intensity was ∼5% of that observed at high reagent concentrations (Figure 11), corrected for the $[Cr(VI)]_0$ value and the path length; and (iv) the absorbance due to Cr(III) species (λ_{max} ∼ 560 nm)[67] became apparent after ∼20 min of reaction (Figure 13). No qualitative differences in time-dependent UV−vis spectra were observed at 22 or 27 °C (the NMR spectroscopic studies in the

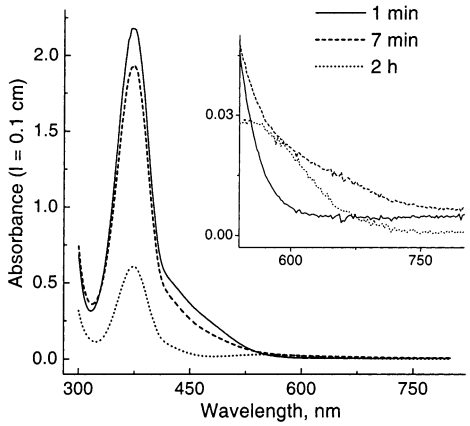

Figure 13. Typical time-dependent UV−vis spectra for the Cr(VI) + GSH reaction under the conditions of Gaggelli et al.[24] ($[Cr(VI)]_0 = 5.0$ mM, $[GSH]_0 = 20.0$ mM, $[GSSG]_0 = 5.0$ mM, pH = 7.4, adjusted with NaOH, in D_2O solution, 22 °C).

previous work[24] were performed at 27 °C, while the ESMS and EPR spectroscopic studies in this work were carried out at 22 °C). Reference in the previous study[24] to the strong absorbance at ∼206 nm, assigned to Cr(V) or Cr(IV) species, is unclear (no experimental data are given), as no such absorbance is mentioned in the literature cited by the authors. The absorbance in this region is dominated by the excess of GSH and GSSG.[8]

The typical X-band EPR spectrum (22 °C) of the reaction mixture at the early stage of reaction (2 min, Figure S10a in Supporting Information) possessed signals at $g_{iso} = 1.9857$ (major signal, $A_{iso}(^{53}Cr) = 7.8 \times 10^{-4}$ cm^{-1}, LW $= 0.8 \times 10^{-4}$ cm^{-1}) and at $g_{iso} = 1.9960$ (LW $= 3.5 \times 10^{-4}$ cm^{-1}). The total area of the Cr(V) EPR signals reached a maximum at ∼7 min (Figure S10b), but the signal with $g_{iso} = 1.9857$ persisted longer (for ∼1 h) as the intensity of both signals decreased (Figure S10a). The time scales for the formation and decay of the Cr(V) species, determined by EPR spectroscopy, corresponded to those for the changes in intermediate absorbance at $\lambda = 600-700$ nm (Figure S10b), which supports the assignment of this absorbance to a Cr(V) species. In summary, a small proportion of Cr(V) intermediates (∼5% of total Cr; predominantly with $g_{iso} = 1.9857$) is formed during the Cr(VI) + GSH reaction at relatively low reagent concentrations ($[Cr(VI)]_0 = 5.0$ mM; $[GSH]_0 = 20$ mM). In contrast, the reaction at higher reagent concentrations ($[Cr(VI)]_0 = 50$ mM; $[GSH]_0 = 0.50$ M) led to practically quantitative (≥95%) formation of Cr(V) intermediates (predominantly with $g_{iso} = 1.9958$). These results are in agreement with the previous EPR spectroscopic[11−13,16] and kinetic[77] studies of the Cr(VI) + GSH reaction.

Typical ESMS data (selected regions) in negative- and positive-ion modes under the conditions of Gaggelli et al.[24] are shown in Figure S11 (Supporting Information). The isotope distribution patterns for the signals due to GSH, GSSG, and Cr complexes in D_2O solutions showed a partial H/D exchange of the labile protons (typical examples are shown in Figure S1c). Signals for the Cr species were detected only in the negative-ion mode (Figure S11a) and corresponded to those with $m/z = -117.4$ and -406.3 (Cr(VI) species, Table 1) at the early stage of the reaction, and to those with $m/z = -424.0$ and -483.6 (Cr(III) species, Table 1) at the later stage. The m/z values of nondeuterated species are shown in Figure S11a for comparison with the ESMS data in H_2O solutions (Figures 1, S2, and S8, and Table 1). No ESMS signals due to Cr(V) species were observed, even at the time when maximal [Cr(V)] was detected by EPR and UV−vis spectroscopy (∼7 min at 22 °C), because of the small amounts of Cr(V) formed (Figures 13 and S10). The ESMS signals in the positive-ion mode were due to Na^+/GSH/GSSG adducts, and no signals at $m/z = +711.1$, previously ascribed to $Cr(V)_2GSH_2$,[24] were detected (Figure S11b).

Discussion

Purity and Structure of the Isolated Cr(V)−GSH Complex. Analytical data on isolated Cr(V)−GSH (Table 2 and Figure 9b,c) corresponded to the formulation of this complex as $Na_3[Cr^VO(LH_2)_2]$ (where LH_5 = GSH), containing coprecipitated Na^+ salts of GSH and GSSG, as well as MeOH and H_2O of crystallization. Coprecipitation of reproducible amounts of GSH and GSSG with $Na_3[Cr^VO(LH_2)_2]$ can be explained by hydrogen bonding between the Cr-bound and unbound peptide molecules.

The absence of significant amounts of Cr in oxidation states other than Cr(V) in the isolated solid was confirmed by several independent observations. Kinetic studies (Figures 11 and 12) showed that the conditions used for the isolation of the Cr(V)−GSH complex corresponded to practically quantitative formation of Cr(V) species. Low temperature EPR spectroscopy (Figure 3) confirmed the absence of detectable amounts of Cr(III) in solid Cr(V)−GSH, as well as the absence of significant photoreduction of Cr(V)−GSH during XAS measurements. The room temperature magnetic moment was also consistent with a pure Cr(V) complex.[26,48] Dissolving the Cr(V)−GSH complex in $ehbaH_2$/ehbaH buffer (0.20 M, pH = 3.5) led to a fast ligand-exchange reaction with the formation of $[Cr^VO(ehba)_2]^-$ (confirmed by EPR spectroscopy), which was subsequently reduced to Cr(III) by GSH with the formation of $[Cr^{IV}O(ehbaH_2)]^0$ as an intermediate (Figure 10).[28,72] If significant amounts of Cr(IV) were present in the isolated solid,[78] the fast ligand-exchange reaction with $ehbaH_2$/ehbaH under these conditions would lead to the formation of $[Cr^{IV}O(ehbaH_2)]^0$, which is easily distinguished from $[Cr^VO(ehba)_2]^-$ by its strong absorbance at 400−600 nm.[71] The formation of $[Cr^{IV}O(ehbaH_2)]^0$ in the presence of excess $ehbaH_2$/ehbaH at pH = 3.5 was previously used to prove and quantify the formation of Cr(IV) intermediates during the decomposition of $[Cr^VO(ehba)_2]^-$.[43] The presence of significant amounts of Cr(VI) in Cr(V)−GSH would lead to the detection of

(77) O'Brien, P.; Ozolins, Z. *Inorg. Chim. Acta* **1989**, *161*, 261−266.

(78) Isolation of a Cr(IV)−GSH complex from the reaction of Cr(VI) with 2 molar equiv of GSH at pH ∼3 has been reported: Liu, K. J.; Shi, X.; Dalal, N. S. *Biochem. Biophys. Res. Commun.* **1997**, *235*, 54−58. However, the results of EPR spectroscopy, ligand-exchange studies, and ESMS show that under these conditions a mixture of Cr(III) and Cr(VI) species is formed.[7,8]

Chart 2. Proposed Structures of Cr(V) Species, Observed by ESMS (Table 1)[a]

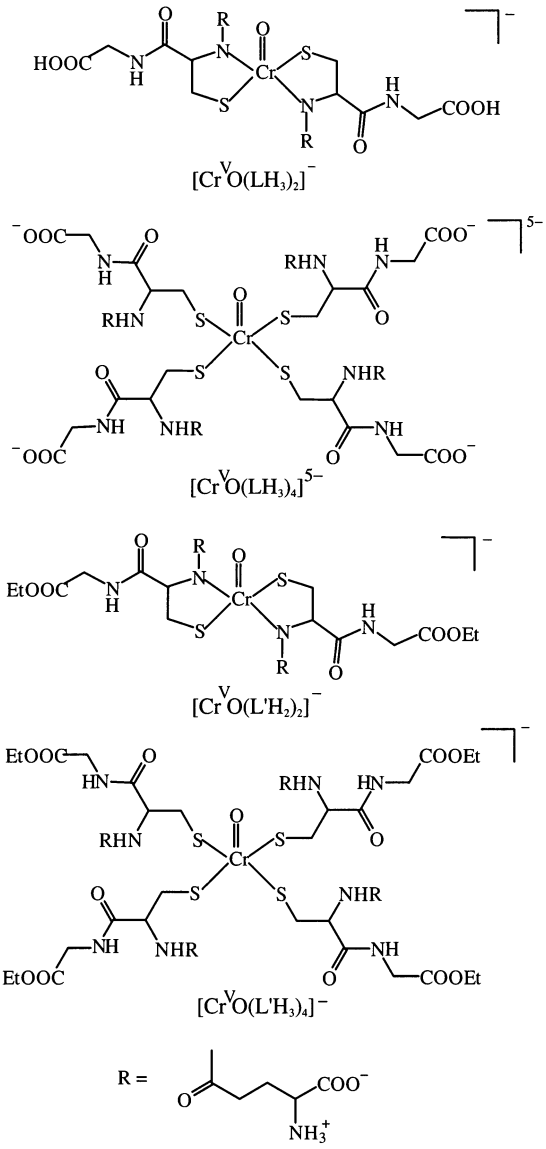

[a] Structures of $[Cr^{V}O(LH_3)_3(LH_4)]^{4-}$ and $[Cr^{V}O(LH_3)_2(LH_4)_2]^{3-}$ correspond to that of $[Cr^{V}O(LH_3)_4]^{5-}$, with one or two Gly carboxylato residues protonated.

Cr(VI) in the decomposition products of the Cr(V)−GSH complex at pH 1−4 (the absence of Cr(VI) under these conditions is shown in Figure 9b), as the rates of Cr(VI) reactions with GSH at this pH range are negligibly low compared with the rates of Cr(V)−GSH decomposition (determined by a standard addition method under the conditions of Figure 9). Finally, only one signal due to a Cr(V) species ($[Cr^{V}O(LH_3)_2]^-$; $m/z = -678.5$) was detected in fresh aqueous solutions of the Cr(V)−GSH complex (Figure 1), while several Cr(V)−GSH species were detected by ESMS in the Cr(VI) + GSH reaction mixture (Figure S8, Table 1). These results show that purity of the solid Cr(V)−GSH samples was suitable for XAS studies, as the presence of an excess of free ligand does not affect the XAS data for a metal complex.[48,58b]

Proposed structures for the Cr(V)−GSH species under the conditions of ESMS (in gas phase, Chart 2) were assigned from comparisons of ESMS data for fresh solutions of the isolated Cr(V)−GSH and Cr(V)−GSHOEt solids, and the Cr(VI) + GSH reaction mixture (Figures 1, S4, and S8 and Table 1). Binding of Cr(V) to deprotonated amido and/or thiolato donors of the Cys residue of GSH in $[Cr^{V}O(LH_3)_2]^-$ complexes and $[Cr^{V}O(LH_3)_4]^{5-}$ (Chart 2) is supported by the results of EPR spectroscopic and ESMS studies of Cr(V) complexes, formed during the reactions of Cr(VI) with GSH-related thiols.[16,63,64] Similar coordination modes have also been proposed (based on the EPR and UV−visible spectroscopic studies) for V(IV) oxo complexes with GSH-related ligands (V(IV) is isoelectronic to Cr(V)).[79−81] The coordination modes proposed for the Cr(V)−GSH species (Chart 2; 1M═O + 2M−S + 2M−N or 1M═O + 4M−S, where M is a metal ion) have been observed in numerous crystal structures of Mo(V) complexes.[82,83] The coordination of GSH as a chelating ligand, involving thiolato and amido donors of the Cys residue, has been established for Pt(II)−GSH complexes in neutral aqueous solutions using multinuclear NMR spectroscopy.[84]

Detection of homologous Cr(V) species, $[Cr^{V}O(LH_3)_2]^-$ and $[Cr^{V}O(L'H_2)_2]^-$, for GSH and GSHOEt, respectively (Figures 1 and S4, and Table 1), indicates that the Gly carboxylato residues in $[Cr^{V}O(LH_3)_2]^-$are protonated under the conditions of ESMS (Chart 2). Deprotonation of these residues in neutral aqueous solutions and in the isolated Cr(V)−GSH complex leads to the structure $Na_3[Cr^{V}O(LH_2)_2]$, in agreement with the analytical data (Table 2 and Figure 8b,c).

The proposed structure of the isolated Cr(V)−GSH complex (**I** in Chart 3) is in agreement with the results of XAS studies (Figures 4−6 and Tables 3 and 4). A distorted trigonal bipyramidal geometry (similar to that of Cr(V) 2-hydroxycarboxylates),[48,62,65] with amido donors in axial positions (Figure 6), has been deduced for the Cr(V)−GSH complex on the basis of MS XAFS calculations (Tables 4, S4, and S5). Such a geometry is in agreement with a relatively intense pre-edge absorbance in the XANES spectrum (Figure 4),[48,58] and with the axial symmetry of the complex, revealed by the solid state Q-band EPR spectroscopy (Figure 2). The three-dimensional structures of the Cr(V)−GSH complexes, determined from MS XAFS fits to the data starting from two independent models (models 2 and 4 in Chart 1 and Table 4), were similar but not equivalent (Table S5). This observation, as well as the observed disorder in the position of the oxo group (reflected in the relatively high σ_i^2 value for this group, Tables 3 and 4), may point to the presence of a mixture of more than one energetically

(79) Dessì, A.; Micera, G.; Sanna, D. *J. Inorg. Biochem.* **1993**, *52*, 275−286.
(80) Baran, E. J. *J. Inorg. Biochem.* **2000**, *80*, 1−10.
(81) Tasiopoulos, A. J.; Troganis, A. N.; Deligiannakis, Y.; Evangelou, A.; Kabanos, T. A.; Woolins, J. D.; Slawin, A. *J. Inorg. Biochem.* **2000**, *79*, 159−166.
(82) Dilworth, J. R. In *Molybdenum: An Outline of its Chemistry and Uses*; Braithwaite, E. R.; Haber, J., Eds.; Elsevier: Amsterdam, 1994; pp 185−250.
(83) Thomson, L. M.; Hall, M. B. *J. Am. Chem. Soc*. **2001**, *123*, 3995−4002.
(84) Berners-Price, S. J.; Kuchel, P. W. *J. Inorg. Biochem.* **1990**, *38*, 305−326.

Chart 3. Structure of the Isolated Cr(V)−GSH Complex (**I**) and Possible Structures of Major Species in the Isolated Cr(III)−GSH (**II**)[a]

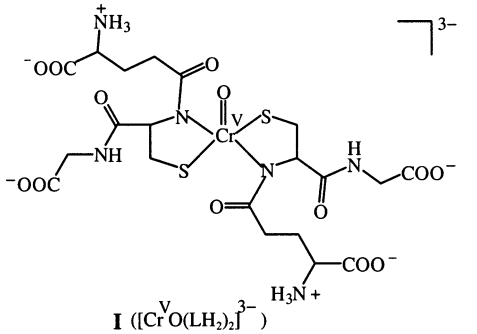

I ($[Cr^{V}O(LH_2)_2]^{3-}$)

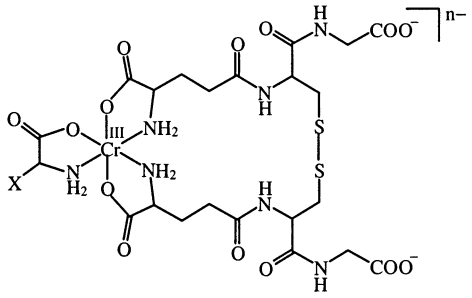

II (X = GSH or GSSG residue; n = 3 or 4)

[a] Structures **I** and **II** may represent mixtures of geometric and/or conformational isomers.

close geometric isomers in the isolated Cr(V)−GSH complex[48,62,65] or slightly different environments for independent complexes in the crystal structure (as is observed for $Na[CrO(ehba)_2]$).[52]

A six-coordinate structure of the solid Cr(V)−GSH (including one oxo, two thiolato, and three deprotonated amido donors, similar to model 6 in Chart 1) was proposed[7] on the basis of preliminary analysis of the XAFS data. However, more detailed SS and MS XAFS analyses, including the data comparison for two different preparations of Cr(V)−GSH, have shown the preference of a five-coordinate model over a six-coordinate one (Tables 4 and S2). The previously proposed six-coordinate structure[7] also disagrees with the results of chemical analyses of isolated Cr(V)−GSH (Table 2 and Figure 8b,c), and with the results of comparative EPR spectroscopic studies of the Cr(V) complexes of GSH and related thiols.[16,63,64] Similar to a well-characterized Cr(V) complex, $[Cr^{V}O(ehba)_2]^-$,[52,58,85] binding of a sixth ligand to **I** is unlikely from steric considerations, given the bulky nature of the substituents (Chart 3).

The Cr═O(oxo) bond in **I** (1.61 Å; determined by MS XAFS calculations; Table 4) is slightly longer than those for most of the known Cr(V) oxo complexes (1.52−1.59 Å)[48,52,58,62] and corresponds (within 0.01 Å experimental error)[44] to those in the crystallographically characterized Cr(VI) thiolato complex, $[Cr^{VI}O_3SR]^-$ (where RSH is 4-bromobenzenethiol).[86] The Cr−N(amido) bonds (1.99 Å, Table 4) in **I** are longer than those for Cr(V) complexes with macrocyclic polyamido ligands (1.91−1.96 Å)[62] and are close to those for Cr(III) peptide complexes (1.96−1.98 Å).[87] In contrast, the Cr−S(thiolato) bonds in **I** (2.31 Å, Table 3) are significantly shorter than those in Cr(III)−Cys complexes (2.37−2.39 Å)[88,89] and are similar to that in the $[Cr^{VI}O_3SR]^-$ complex (2.30 Å).[86] Shortening of Cr−S bonds and elongation of Cr−N and Cr═O bonds in **I** are consistent with a significant electron withdrawal from S atoms of the ligands by Cr(V), which is evident from a decreased edge energy in the XANES spectrum of **I**, compared with that of $[Cr^{V}O(ehba)_2]^-$ (Figure 4). A significant transfer of electron density from donor atoms to metal centers was also observed in Cr(V) catecholato complexes,[58b] as well as in Mo(VI/V/IV) thiolato complexes.[90,91]

Structures of Cr(III) Products of the Cr(VI) + GSH Reaction. The results of SS XAFS analysis for the isolated Cr(III)−GSH solid (Table 3) are consistent with Cr(III) binding to three chelating (carboxylato + amino) groups of γ-Glu residues in GSH or GSSG. The bond lengths (1.93 Å for carboxylato donors and 2.05 Å for amino donors; Table 3) are in good agreement with the corresponding values for Cr(III) complexes with amino acid and peptides.[67,87−89,92]

At least four different signals due to Cr(III) species were detected in the isolated Cr(III)−GSH compound by ESMS (Figure S2); compositions of three of them ($[Cr^{III}(LLH_4)(LLH_6)]^{3-}$, $[Cr^{III}(LLH_4)(LH_4)]^{2-}$, and $[Cr^{III}(LLH_5)(LH_4)]^-$ in Table 1) are consistent with Cr(III) binding to γ-Glu residues of GSSG and GSH (general structure **II** in Chart 3). The same Cr(III) species were detected during the decomposition of the isolated Cr(V)−GSH complex in aqueous solution (Figure 1), as well as in the products of the Cr(VI) + GSH reaction at high or low reagent concentrations (Figures S8 and S11). Binding of both γ-Glu residues in GSSG to a single metal ion (as in **II**) has been proposed for the complexes of this ligand with Co(II), Ni(II), Cu(II), Zn(II), and V(V) in neutral aqueous solutions (based on potentiometric and UV−vis spectroscopic studies),[93,94] and such coordination is likely to be facilitated by a 19-membered ring formed by the ligand.[93] The fourth Cr(III) species, detected by ESMS ($[Cr^{III}(LH)]^-$, Table 1), is probably a fragmentation product of the initial Cr(III) complexes **II**, formed under ESMS conditions.[35,36]

Formation of oxo- or hydroxo-bridged oligonuclear Cr(III) species with amino acid ligands in neutral aqueous solutions

(85) Bose, R. N.; Fonkeng, B.; Barr-David, G.; Farrell, R. P.; Judd, R. J.; Lay, P. A.; Sangster, D. F. *J. Am. Chem. Soc.* **1996**, *118*, 7139−7144.
(86) Mazurek, W.; Fallon, G. D.; Nichols, P. J.; West, B. O. *Polyhedron* **1990**, *5*, 777−779.
(87) Murdoch, C. M.; Cooper, M. K.; Hambley, T. W.; Hunter, W. N.; Freeman, H. C. *J. Chem. Soc., Chem. Commun.* **1986**, 1329−1331.
(88) De Meester, P.; Hodgson, D. J.; Freeman, H. C.; Moore, C. J. *Inorg. Chem.* **1977**, *16*, 1494−1498.
(89) Madafiglio, K.; Manning, T. M.; Murdoch, C. M.; Tulip, W. R.; Cooper, M. K.; Hambley, T. W.; Freeman, H. C. *Acta Crystallogr., Sect. C* **1990**, *46*, 554−561.
(90) Izumi, Y.; Glaser, T.; Rose, K.; McMaster, J.; Basu, P.; Enemark, J. H.; Hedman, B.; Hodgson, K. O.; Solomon, E. I. *J. Am. Chem. Soc.* **1999**, *121*, 10035−10046.
(91) Helton, M. E.; Gebhart, N. L.; Davies, E. S.; McMaster, J.; Garner, C. D.; Kirk, M. L. *J. Am. Chem. Soc.* **2001**, *123*, 10389−10390.
(92) Headlam, H. A.; Weeks, C. L.; Turner, P.; Hambley, T. W.; Lay, P. A. *Inorg. Chem.* **2001**, *40*, 5097−5105.
(93) Várnagy, K.; Sóvagó, I.; Kozlowski, H. *Inorg. Chim. Acta*, **1988**, *151*, 117−123.
(94) Costa Pessoa, J.; Tomaz, I.; Kiss, T.; Buglyo, P. *J. Inorg. Biochem.* **2001**, *84*, 259−270.

is common,[67] but no evidence for such species has been found in the ESMS of Cr(III)−GSH (Figure S2, Table 1). However, a significant peak in the FT XAFS spectrum at ∼3.2 Å (uncorrected for the phase shift, Figure S6b) may indicate the presence of at least minor species with Cr−O−Cr bonds in solid Cr(III)−GSH.[92] No such peak was observed in the FT XAFS spectra of Cr(V)−GSH (Figures 5 and S6a), consistent with the mononuclear structure **I** of this complex.

Nature of the Species Observed by Gaggelli et al.[24] Kinetic studies of the Cr(VI) + GSH reaction under the reported conditions[24] (Figures 13, S10, and S11) showed that Cr(V) was formed as a minor intermediate (maximum of ∼5% of total Cr). The [Cr(V)] increased in the first ∼7 min of the reaction and then decayed over ∼1 h (22 °C). As Cr(V) is an unstable intermediate in the Cr(VI) + GSH reaction,[21,77] time-dependent studies are essential to relate any phenomena (such as signal broadening in NMR spectra or detection of certain ESMS signals)[24] to the formation of Cr(V) species. No such studies were mentioned by Gaggelli et al., and no details were given for the time points at which the reported results were observed.[24] However, our kinetic data (Figures 13, S10, and S11) show that Cr(III) was the dominant paramagnetic species during the Cr(VI) + GSH reaction under the reported conditions.[24] Therefore, the results of paramagnetic NMR spectroscopy[24] are likely to describe the structures of the formed Cr(III) products, rather than Cr(V) intermediates. Although pure mononuclear Cr(III) complexes usually possess very broad and poorly resolved ^{1}H NMR signals in solutions,[95] relatively small amounts of Cr(III) species formed at the initial stages of the Cr(VI) + GSH reaction in the presence of excess GSH and GSSG will lead to a partial broadening and shift of the signals, as observed in the previous work.[24] Notably, polynuclear Cr(III) complexes often possess relatively sharp and well-resolved signals in ^{1}H NMR spectra,[95−97] which may support the formation of dinuclear Cr(III) species under the studied conditions.[24] According to the NMR data,[24] Cr(III) in such products is likely to be bound to carboxylato and amino moieties of γ-Glu residues in GSH or GSSG, but thiolato moieties of GSH are unlikely to be involved in Cr(III) binding. This suggestion is supported by our ESMS and XAS studies of Cr(III) products of the Cr(VI) + GSH reactions (see preceding discussion). In contrast, attempts to apply a structure proposed by Gaggelli et al. (containing carboxylato, amino, and H_2O donors, but no oxo or thiolato donors),[24] to SS XAFS calculations of the first coordination shell in the isolated Cr(V)−GSH complex, led to very poor fits (R > 40%, a typical example is shown in column 4, Table S2).

The assignment of the ESMS signal with $m/z = +711.2$ to $[Cr^V_2(GSH)_2]$ species[24] (apparently the only Cr species detected in the reaction mixture by ESMS) poses several questions. First, no results of negative-ion ESMS were presented in the previous work.[24] By contrast, in our ESMS studies of Cr(V)−GSH and related systems (Table 1 and Figures 1, S1−S4, S8, and S11), all Cr species were observed in the negative-ion mode. Second, the ESMS signal with $m/z = +711.2$ (for the main peak in the isotopic distribution) and 1+ charge (p 4 in Supporting Information to the published work)[24] can be attributed to $[Cr^{III}_2(LLH_3)]^+$ species (where LLH_8 = GSSG). The $[Cr^V_2(GSH)_2]$ structure proposed by the authors[24] would lead to the observation of multiply charged Cr species in the ESMS. An attempt was made to solve this controversy by suggesting that the Cr(V) species are reduced (via H^- binding) under the ESMS conditions (p 3 in Supporting Information to the published work);[24] however, no justification of this hypothesis was given. Indeed, positive-ion ESMS provides oxidizing, rather than reducing, conditions.[35] Third, there is a clear disagreement in the relative intensities of the satellite peaks in isotopic distributions for the observed and simulated ESMS signals (pp 4−5 in Supporting Information to the published work), which was not explained by the authors.[24] Finally, the attribution of two discrete signals with $m/z = +711.2$ and +717.0 to protonated and deuterated forms of the studied species (in D_2O solution)[24] is incorrect, because the H/D exchange would lead to detection of a continuous array of signals with different H/D ratios (typical examples are shown in Figure S1c). We were unable to observe the species with $m/z = +711.2$ in the positive-ion ESMS under the reported conditions[24] (Figure S11b). Reasons for this are unclear, as no experimental details of ESMS were given.[24]

In summary, our experimental results and analysis of the published data[24] establish that the postulated $[Cr^V_2(GSH)_2]$ dimer is not a major product (or intermediate) of the Cr(VI) + GSH reaction at relatively low reagent concentrations. This does not exclude the possibility of formation of a dimeric Cr(V) complex as a minor intermediate (undetectable by ESMS) under the conditions of Gaggelli et al.[24] Such a complex may be responsible for the observed signal with $g = 1.93$ in high-frequency EPR spectra (282 GHz) of the reaction mixture at 10 K.[24] Dimeric species, involving a spin coupling of two Cr(V) centers with $S = {}^1/_2$ (as proposed for $[Cr^V_2(GSH)_2]$),[24] are expected to be EPR-silent at room temperature.[62] Unfortunately, no comparison of EPR spectra at low and ambient temperatures has been reported.[24] Recently, a dimeric Cr(V)−Ala complex (involving Cr(V) coordination to carboxylato and amino groups) has been isolated from the Cr(VI) + Ala reaction in MeOH, and its structure has been determined by ESMS and XAS.[92] However, our EPR-spectroscopic studies (X-band, ∼9.46 GHz) at 10 K (Figure 3), as well as the results of ESMS (Figure 1 and Table 1) and XAFS spectroscopy (Figure 5 and Tables 3 and 4), did not provide any evidence for the presence of significant amounts of dimeric Cr(V) species in the isolated Cr(V)−GSH complex.

Solution Structures, Reactivities, and Possible Biological Roles of Cr(V)−GSH Complexes. The EPR spectroscopic and ESMS data suggest the presence of several types of Cr(V)−GSH species in solutions. Thus, the reaction of Cr(VI) (50.0 mM) with a 10-fold molar excess of GSH at

(95) Kingry, K. F.; Royer, A. C.; Vincent, J. B. *J. Inorg. Biochem.* **1998**, *72*, 79−88.
(96) Glass, M. M.; Belmore, K.; Vincent, J. B. *Polyhedron* **1993**, *12*, 133−140.
(97) Ellis, T.; Glass, M.; Harton, A.; Folting, K.; Huffman, J. C.; Vincent, J. B. *Inorg. Chem.* **1994**, *33*, 5522−5527.

pH = 7.0 produces a mixture of bis-thiolato ($[Cr^{V}O(LH_2)_2]^{3-}$, **I**) and tetra-thiolato ($[Cr^{V}O(LH_3)_4]^{5-}$) intermediates (Charts 2 and 3, Table 1, and Figure S8). However, when a large volume of MeOH is added to the reaction mixture during the isolation of Cr(V)−GSH,[21] only **I** is precipitated (as shown by ESMS, Figure 1). This can be explained by a difference in the solubility of the bis- and tetra-thiolato complexes in MeOH, and/or a shift of equilibrium toward the bis-thiolato form, as [GSH] decreases after the addition of MeOH.

The main signal (g_{iso} = 1.9960) in the EPR spectrum of an aqueous solution of the isolated Cr(V)−GSH complex (Figure 7a) is assigned to **I**, as similar *g* values were observed in the solid-state EPR spectra of **I** (Figures 2 and 3), indicating that the five-coordinate structure determined for the solid state is retained in solution. A comparison with the EPR spectrum of the reaction mixture (Figure S9a, $[Cr(VI)]_0$ = 50 mM, $[GSH]_0$ = 0.50 M, pH = 7.0) suggests that the g_{iso} values for **I** and $[Cr^{V}O(LH_3)_4]^{5-}$ are close (1.9958−1.9960), which is in agreement with the similar g_{iso} values for Cr(V) complexes with thiolato or amido donors.[8,19,62] The EPR spectra (Figures 7 and S9), in agreement with the kinetic data (Figure 8), indicate that the decomposition of **I** (g_{iso} = 1.9960) in aqueous solutions passes through other Cr(V) intermediates (g_{iso} = 1.9857, 1.9770, and 1.9725). The appearance of new Cr(V) species with g_{iso} values lower than that for **I**, in solutions of Cr(V)−GSH complexes (Figures 6 and S9), is likely to be due to the partial replacement of thiolato and amido donors in **I** with carboxylato, amino, and H_2O-derived donors.[8,19,98] Such Cr(V) species are likely to form (as reactive steady-state intermediates) en route to the Cr(III) products (such as **II** in Chart 3), as the structures of kinetically inert Cr(III) products reflect the structures of labile Cr(V/IV) intermediates from which they are generated in the course of Cr(VI) reductions.[42] Structures of the Cr(V) species, giving rise to minor EPR signals in the solutions of Cr(V)−GSH (g_{iso} = 1.9857, 1.9825, 1.9970, and 1.9725, Figures 6 and S9), have been assigned from comparative EPR-spectroscopic studies of Cr(V) complexes of GSH and related thiols.[16] This will be the subject of a separate article.[63]

The existence of an equilibrium between bis- and tetra-thiolato forms of Cr(V)−GSH in neutral aqueous solutions in the presence of excess GSH (Chart 2, Table 1, and Figure S8) suggests easy protonation of amido donors in **I**, in agreement with relatively long Cr−N bonds in this complex (1.99 Å, Table 3). A relatively weak Cr−N(amido) binding may explain the absence of resolved superhyperfine (SHF) structure due to ^{14}N donors in the solution EPR spectra of **I** (Figure 7a), in contrast with many known Cr(V) complexes with N-donor ligands, where well-resolved SHF structures due to ^{14}N ($a_N = (2.2-3.3) \times 10^{-4}$ cm^{-1}) are observed.[8,19,62] However, some examples of unresolved SHF structures due to N-donors in EPR spectra of Cr(V) complexes are known (e.g., imine donors in 1,10-phenanthroline ligand,[99,100] or amino donors in amino acid or peptide[98] ligands), resulting in relatively broad EPR signals of Cr(V) species (LW = (3−5) × 10^{-4} cm^{-1}), similar to that observed for **I** (g_{iso} = 1.9960; Figure 7a). Easy protonation of amido donors in **I** is also consistent with rapid decomposition of this complex in weakly acidic aqueous media (Figure 9a), which is in marked contrast with the stability−pH relationship for Cr(V) 2-hydroxycarboxylato complexes.[48,68]

Decomposition of **I** at pH = 1−13 occurs predominantly via a ligand oxidation mechanism (eq 2, Figure 8), consistent with a significant electron transfer from S atoms of the ligands to Cr(V) (Figure 4). Such electron transfer indicates a likely intramolecular mechanism of **I** reduction to Cr(III) products.[32] For instance, addition of GSH (up to 5.0 mM) to solutions of **I** ([Cr] = 1.0 mM) at pH = 1−13 did not cause significant changes in the rates of Cr(V) decomposition, and I^- was not oxidized to I_2 by **I** at pH = 0−3 (see Results).

Several model Cr(V) complexes with nonbiological ligands (most often $[Cr^{V}O(ehba)_2]^-$) have been used to study the roles of Cr(V) complexes in Cr(VI)-induced genotoxicity.[5,7,8,25] Further understanding of these roles requires a knowledge of the structures and reactivities of Cr(V) species that are likely to form intracellularly, including Cr(V)−GSH complexes. The ability of $[Cr^{V}O(ehba)_2]^-$ to induce oxidative DNA cleavage through direct Cr(V)−DNA interactions has been demonstrated.[7,8,25] However, the kinetic data for the decomposition of **I** (Figures 8 and 9) show that Cr(V)−GSH complexes are likely to form Cr(III) products through intramolecular redox reactions[32] and thus are less likely to react with "external" reductants such as DNA. The previously reported O_2-dependent DNA cleavage in vitro, induced by the isolated Cr(V)−GSH complex,[101,102] may be caused by the Cr(VI) + GSH system, which is formed during the decomposition of the Cr(V) species in neutral aqueous solutions (Figure 9b,c), and is well-known to induce oxidative DNA cleavage in the presence of O_2.[8,102] Comparative kinetic studies of decomposition of the Cr(V)−GSH complex and DNA cleavage induced by Cr(V)−GSH are required to resolve these possibilities.

Of greater biological importance are probably the ligand-exchange reactions of Cr(V)−GSH complexes with carbohydrates, such as D-glucose[103,104] or sialoglycoproteins,[105] and other intracellular ligands, such as 2-hydroxycarboxylates.[65,105] A fast ligand-exchange reaction of **I** with a 2-hydroxycarboxylato ligand, ehba, has been observed in slightly acidic aqueous media (Figure 9), which is relevant to the uptake and reduction of insoluble Cr(VI) compounds

(98) Headlam, H. A.; Lay, P. A. *Inorg. Chem.* **2001**, *40*, 78−86.
(99) Dillon, C. T.; Lay, P. A.; Bonin, A. M.; Dixon, N. E.; Sulfab, Y. *Aust. J. Chem.* **2000**, *53*, 411−424.
(100) Sulfab, Y.; Nasreldin, M. *Transition Met. Chem.* **2001**, *26*, 147−149.
(101) Kortenkamp, A.; Oetken, G.; Beyersmann, D. *Mutat. Res.* **1990**, *232*, 155−161.
(102) Kortenkamp, A.; Casadevall, M.; Faux, S. P.; Jenner, A.; Shayer, R. O. J.; Woodbridge, N.; O'Brien, P. *Arch. Biochem. Biophys.* **1996**, *329*, 199−207.
(103) (a) Irwin, J. A. Ph.D. Thesis, University of Sydney, 1997. (b) Irwin, J. A.; Hanson, G.; Lay, P. A. To be submitted.
(104) Branca, M.; Dessí, A.; Kozlowski, H.; Micera, G.; Swiatek, J. *J. Inorg. Biochem.* **1990**, *39*, 217−226.
(105) Codd, R.; Lay, P. A. *J. Am. Chem. Soc.* **2001**, *123*, 11799−11800.

by the cells through phagocytosis.[7,8,65] Carbohydrates possess high affinity for Cr(V) in neutral aqueous media,[103−105] and they are more abundant in biological systems than any other type of ligands.[106] Reduction of Cr(VI) with GSH in vitro in the presence of excess D-glucose or other 1,2-diolato ligands at pH ≥ 7 leads predominantly to the formation of Cr(V)−carbohydrate complexes.[65,103−105] Therefore, the Cr(V)−GSH complexes, initially formed during the intracellular reduction of Cr(VI), are likely to be present in small steady-state concentrations compared with the Cr(V)−carbohydrate complexes. This in agreement with the results of EPR spectroscopic studies of whole live animals, treated with Cr(VI), where only Cr(V)−carbohydrate complexes were detected.[7,8,107]

Acknowledgment. Financial support of this work by an Australian Research Council (ARC) grant (to P.A.L.), AusAID Ph.D. Scholarship (to L.Z.), and ARC RIEFP grants for ESMS, EPR, and stopped-flow equipment and the ten-element Ge detector is gratefully acknowledged. X-ray absorption spectroscopy was performed at the Australian National Beamline Facility (ANBF) in Tsukuba with support from the Australian Synchrotron Research Program, which is funded by the Commonwealth of Australia under the Major National Research Facilities program. The authors thank Drs. Garry Foran and James Hester (ANBF) and Mr. Peter Barnard (University of Sydney) for the assistance with XAS, Dr. Ming Xie (University of Sydney) for the assistance with low temperature and Q-band EPR specroscopies, and Dr. Sandra Moussa (University of Sydney) for the assistance with TGA.

Supporting Information Available: Tables showing the details of XAFS data analyses and figures showing typical results of SS XAFS analyses, ESMS, TGA, and EPR spectroscopy. This material is available free of charge via the Internet at http://pubs.acs.org.

IC020621O

(106) Gyurcsik, B.; Nagy, L. *Coord. Chem. Rev.* **2000**, *203*, 81−149.
(107) Liu, K. J.; Shi, X.; Jiang, J.; Goda, F.; Dalal, N.; Swartz, H. M. *Ann. Clin. Lab. Sci.* **1996**, *26*, 176−184.